

# 1 High-resolution projections of ambient heat for major European cities using 2 different heat metrics

3 Clemens Schwingshackl<sup>1,2</sup>, Anne Sophie Daloz<sup>2</sup>, Carley Iles<sup>2</sup>, Kristin Aunan<sup>2</sup>, and Jana Sillmann<sup>3,2</sup>

4 <sup>1</sup>Department of Geography, Ludwig-Maximilians-Universität München, Munich, Germany

5 <sup>2</sup>Center for International Climate Research (CICERO), Oslo, Norway

6 <sup>3</sup>Center for Earth System Research and Sustainability (CEN), University of Hamburg, Hamburg, Germany

7 *Correspondence to:* Clemens Schwingshackl ([c.schwingshackl@lmu.de](mailto:c.schwingshackl@lmu.de))

8 **Abstract.** Heat stress in cities is projected to strongly increase due to climate change. The associated health risks will be  
9 exacerbated by the high population density in cities and the urban heat island effect. However, impacts are still uncertain,  
10 which is among other factors due to the existence of multiple metrics for quantifying ambient heat and the typically rather  
11 coarse spatial resolution of climate models. Here we investigate projections of ambient heat for 36 major European cities based  
12 on a recently produced ensemble of regional climate model simulations for Europe (EURO-CORDEX) at 0.11° spatial  
13 resolution (~12.5 km). The 0.11° EURO-CORDEX ensemble provides the best spatial resolution currently available from an  
14 ensemble of climate model projections for the whole of Europe and makes it possible to analyse the risk of temperature  
15 extremes and heatwaves at the city-level. We focus on three temperature-based heat metrics — yearly maximum temperature,  
16 number of days with temperatures exceeding 30 °C, and Heat Wave Magnitude Index daily (HWMId) — to analyse projections  
17 of ambient heat at 3 °C warming in Europe compared to 1981-2010 based on climate data from the EURO-CORDEX ensemble.  
18 The results show that southern European cities will be mostparticularly affected by high levels of ambient heat, but depending  
19 on the considered metric, cities in central, eastern, and northern Europe may also experience substantial increases in ambient  
20 heat. In several cities, projections of ambient heat vary considerably across the three heat metrics, indicating that estimates  
21 based on a single metric might underestimate the potential for adverse health effects due to heat stress. Nighttime ambient  
22 heat, quantified based on daily minimum temperatures, shows similar spatial patterns as daytime conditions, albeit with  
23 substantially higher HWMId values. The identified spatial patterns of ambient heat are generally consistent with results from  
24 global Earth system models, though with substantial differences for individual cities. Our results emphasise the value of high-  
25 resolution climate model simulations for analysing climate extremes at the city-level. At the same time, they highlight that  
26 improving the currentlypredominantly rather simple representations of urban areas in climate models would make their  
27 simulations even more valuable for planning adaptation measures in cities. Further, our results stress that using complementary  
28 metrics for projections of ambient heat gives important insights into the risk of future heat stress that might otherwise be  
29 missed.

## 30 1 Introduction

31 Global heat stress is projected to strongly increase in the future due to climate change (Gasparrini et al., 2017; Vargas  
32 Zeppetello et al., 2022; Zheng et al., 2021; Schwingshackl et al., 2021; Freychet et al., 2022), and already nowadays record-  
33 breaking high temperatures are observed more and more often around the world, such as in Canada in summer 2021 ~~or in~~  
34 ~~China and Europe in summer 2022.~~(White et al., 2023) or in China and Europe in summer 2023 (Zachariah et al., 2023). Heat  
35 stress can have severe implications for human health, the economy, and the society as a whole (e.g., McMichael et al., 2006;  
36 Gasparrini et al., 2015; Yang et al., 2021; Alizadeh et al., 2022; Orlov et al., 2021), as it can lead to decreased levels of comfort  
37 and reduced labour productivity (Orlov et al., 2021; García-León et al., 2021), enhanced socioeconomic inequalities (Alizadeh  
38 et al., 2022), and increased morbidity and mortality (Gasparrini et al., 2015). Moreover, as the health risk associated with heat  
39 stress is not uniform within the population, heatwaves and extreme temperatures pose a larger threat to those who are most  
40 vulnerable to elevated temperatures, particularly to children, older adults, and persons with pre-existing conditions (Lundgren  
41 et al., 2013).

42 Various metrics have been developed with the aim to capture the characteristics of heat extremes, including heatwaves, and  
43 their potential evolution in the future ~~(e.g., Perkins and Alexander, 2013; Perkins, 2015).~~(e.g., Perkins and Alexander, 2013;  
44 Perkins, 2015; de Freitas and Grigorieva, 2017). Several of these indicators are based solely on temperature, while others  
45 consider additional factors, such as humidity, solar radiation, or wind speed to estimate heat exposure (de Freitas and  
46 Grigorieva, 2017). In the following, we focus on temperature-based metrics, given that many epidemiological studies found  
47 temperature to be the dominant factor for adverse health effects (Armstrong et al., 2019; Kent et al., 2014; Vaneckova et al.,  
48 2011). Future changes in heat and heat extremes are frequently quantified by the change in temperature (e.g., mean or  
49 maximum near-surface air temperature) between a historical reference period and future periods ~~(Sillmann et al., 2013; IPCC,~~  
50 ~~2021; Coppola et al., 2021)~~(Sillmann et al., 2013; IPCC, 2021; Coppola et al., 2021). Other studies used the number of days  
51 per year during which certain thresholds are exceeded (e.g., Casanueva et al., 2020; Schwingshackl et al., 2021; Zhao et al.,  
52 2015). Likewise, different metrics have been introduced to quantify heatwaves, often based on percentile-based thresholds  
53 (e.g., Fischer and Schär, 2010; Suarez-Gutierrez et al., 2020; Perkins-Kirkpatrick and Lewis, 2020). The Heat Wave Magnitude  
54 Index daily (HWMId, Russo et al., 2015) integrates both the magnitude and the length of a heatwave into a single metric to  
55 quantify the heatwave severity. HWMId was applied by several studies to analyse the future risk of heatwaves (e.g., Dosio et  
56 al., 2018; Russo et al., 2017; Forzieri et al., 2016; Zittis et al., 2021). Depending on the considered metric, the projected spatial  
57 patterns of ambient heat projections may vary considerably, highlighting that assessing the future risk from heat stress requires  
58 considering a portfolio of metrics.

59 The health risk from heat stress is not spatially homogeneous – neither globally nor within a country or a region – owing to  
60 several factors, including variations in local climate conditions, local climate feedbacks (e.g., due to albedo, soil moisture), or  
61 differences in the social environment (e.g., population density, socioeconomic conditions). Temperatures are often amplified  
62 in cities due to the predominance of impervious surfaces and the multitude of anthropogenic heat sources. The resulting urban

63 heat island (UHI) effect leads to higher levels of ambient heat in cities compared to surrounding areas (e.g., Heaviside et al.,  
64 2017). In Europe, our region of study, about 75% of the population lives in urban areas (UN-Habitat, 2011) and the urban  
65 population is projected to grow even further in the future along with an ageing trend (Smid et al., 2019). Larger metropolitan  
66 areas in Europe will become more vulnerable to extreme heat in the coming decades (Smid et al., 2019) and heat mortality in  
67 European cities is projected to significantly increase (Karwat and Franzke, 2021). Cities in Europe or elsewhere are thus  
68 becoming climate hotspots in terms of climate change (Zheng et al., 2021) but also for adaptation and innovation (IPCC, 2022)  
69 due to the need for adequate strategies to address climate change adaptation. Preventing adverse health outcomes from heat  
70 stress and designing appropriate and effective adaptation measures requires accurate projections and estimates of heatwaves  
71 and temperature extremes. Recently, climate model simulations have reached a spatial resolution high enough to provide such  
72 projections at the city-level.

73 Analyses of climate and climate change in cities face the challenge of delivering results on spatial resolutions that are high  
74 enough to be relevant for cities while robustly estimating the risk of extreme events. Urban canopy layer models, which can  
75 resolve cities at scales of ~100 m or even higher, can deliver great spatial details of cities (e.g., Masson et al., 2020), with the  
76 trade-off that often only a limited number of cities are examined (e.g., Goret et al., 2019; Krayenhoff et al., 2020). Analyses  
77 with urban canopy layer models coupled to climate models often rely on data from a single or a few climate models and are  
78 thus not able to adequately incorporate climate variability to robustly quantify the probability of extreme events. On the other  
79 hand, climate model simulations can be used to quantify climate variability and the risk of extreme events in multiple cities.  
80 Guerreiro et al. (2018) used simulations by general circulation models (GCMs) from the Climate Model Intercomparison  
81 Project phase 5 (CMIP5) to investigate heatwave projections in European cities. However, GCMs ~~do not~~cannot fully depict  
82 local urban climate conditions as the spatial resolution of GCMs (~100 km) is much coarser than that of urban ~~models and~~  
83 ~~GCMs generally lack a representation of urban areas.~~canopy layer models. To provide higher spatial resolution and to  
84 overcome some of the limitations of GCMs, dynamical downscaling by regional climate models is frequently applied. This  
85 approach has been used multiple times to investigate individual cities with a single model (e.g., Argueso et al., 2015; Chapman  
86 et al., 2019; Keat et al., 2021; Kusaka et al., 2012; Li and Bou-Zeid, 2013; Ramamurthy and Bou-Zeid, 2017; Wouters et al.,  
87 2017) but rarely for analysing climate conditions in a large number of cities and/or with an ensemble of models (e.g., Sharma  
88 et al., 2019; Smid et al., 2019; Junk et al., 2019). For Europe, an ensemble based on regional climate models (RCMs) from the  
89 European branch of the Coordinated Regional Downscaling Experiment (EURO-CORDEX; Jacob et al., 2013; Vautard et al.,  
90 2021) is available, providing simulations at a resolution of 0.11° (EUR-11, ~12.5 km), which is fine enough to analyse climate  
91 conditions in major European cities at the city-level: as typically at least one model grid cell falls within the extent of each  
92 major European city. The EUR-11 simulations were evaluated by Coppola et al. (2021) and Vautard et al. (2021) who showed  
93 that the ~~EURO-CORDEX~~ simulations reproduce well the observed spatial temperature distribution in Europe, despite a general  
94 cold bias of summer temperatures of around 1 °C to 2 °C compared to observation-based data from E-OBS (Cornes et al.,  
95 2018) in large parts of Europe. Hot biases of extreme temperatures (i.e., hottest five consecutive days) in mountainous regions  
96 are reduced in EURO-CORDEX compared to CMIP5, while a cold bias remains in central and northern Europe and a warm

97 bias in southern Europe (Iles et al., 2020). Lin et al. (2022) evaluated the representation of HWMId in a subset of the EURO-  
98 CORDEX ensemble against reanalysis data, finding overall good agreement between both datasets and highlighting the added  
99 value of RCMs compared to the driving GCMs for representing small-scale features.

100 EURO-CORDEX simulations have been used to examine how temperatures and ambient heat are projected to increase in the  
101 future throughout Europe (Vautard et al., 2013; Molina et al., 2020; Coppola et al., 2021) and for a small group of European  
102 cities (Junk et al., 2019; Langendijk et al., 2019; Burgstall et al., 2021), showing that urban areas will be strongly affected by  
103 rising temperatures. The different studies used varying sets of metrics, different model ensembles, and different selections of  
104 cities. Smid et al. (2019) analysed HWMId projections for European capitals based on eight EURO-CORDEX models at 0.11°  
105 resolution, focusing on the metropolitan areas around the capitals. They found highest HWMId increases in southern European  
106 cities and, additionally, they highlight that exposure to heatwaves also strongly depends on population density. Junk et al.  
107 (2019) analysed projections of several heatwave metrics defined by the Expert Team on Climate Change Detection and Indices  
108 (ETCCDI) for London, Luxembourg, and Rome based on 11 EURO-CORDEX models at 0.11° resolution. The considered  
109 heatwave metrics project strongest increases for Rome, except for the number of heatwaves per year, which the authors explain  
110 by the increasing length of heatwaves, reducing their number. Using wet-bulb globe temperature (WBGT) as a heat metric,  
111 Casanueva et al. (2020) analysed exceedances of WBGT thresholds ~~of~~ above 26 °C and 28 °C in Europe based on an ensemble  
112 of 39 EURO-CORDEX models (using simulations at both 0.11° and 0.44° resolution). Future exceedances of WBGT>28 °C  
113 are projected to be highest in southern Europe, followed by central Europe, while exceedance rates are negligible in northern  
114 Europe. Based on CMIP5 GCMs, Guerreiro et al. (2018) found that strongest increases in heatwave days are projected for  
115 southern European cities along with substantial increases in coastal cities in northern Europe, while maximum temperatures  
116 of heatwaves are projected to rise most strongly in central Europe.

117 Here we build on these studies and use simulations by 72 GCM-RCM model combinations of the 0.11° EURO-CORDEX  
118 ensemble to assess projections of ambient heat for 36 major European cities. We focus on ~~near-surface air~~ temperature and  
119 compare three metrics: changes in yearly maximum near-surface air temperature, the number of days per year on which daily  
120 maximum ~~temperatures exceed~~ near-surface air temperature exceeds 30 °C, and HWMId. To evaluate potential differences in  
121 projections for daytime and nighttime conditions, we additionally consider daily minimum near-surface air temperature. We  
122 first analyse how well the EURO-CORDEX ensemble reproduces the measured temperature distributions in the selected cities  
123 compared to reanalysis and observation-based data. Further, we quantify how ambient heat is projected to evolve in these cities  
124 under global warming according to the three considered heat metrics. Finally, we evaluate how the choice of metrics affects  
125 projections of ambient heat, which can give relevant insights for designing appropriate adaptation measures to counteract  
126 health risks from ambient heat. A holistic analysis of the health risk from heat stress comprises the factors heat-related hazards,  
127 heat exposure, and vulnerability to heat. We focus on the hazard from extreme heat by employing the three heat metrics,  
128 acknowledging that exposure and vulnerability can also vary strongly across cities (Smid et al., 2019; Sera et al., 2019;  
129 Gasparri et al., 2015).

## 130 2 Data and Methods

### 131 2.1 Data

#### 132 2.1.1 Cities

133 We include 36 major European cities in our analysis. These comprise all European cities with a population of more than 1.2  
134 million, and all European capitals with more than 500,000 inhabitants. We register the coordinates and elevation of each city,  
135 and whether it is located close to the sea (see Supplementary Table S1). A city is considered to be located close to the sea if it  
136 is directly adjacent to the sea. The complete list of cities and their geographic locations are indicated in Figure 1a.

#### 137 2.1.2 Climate model data

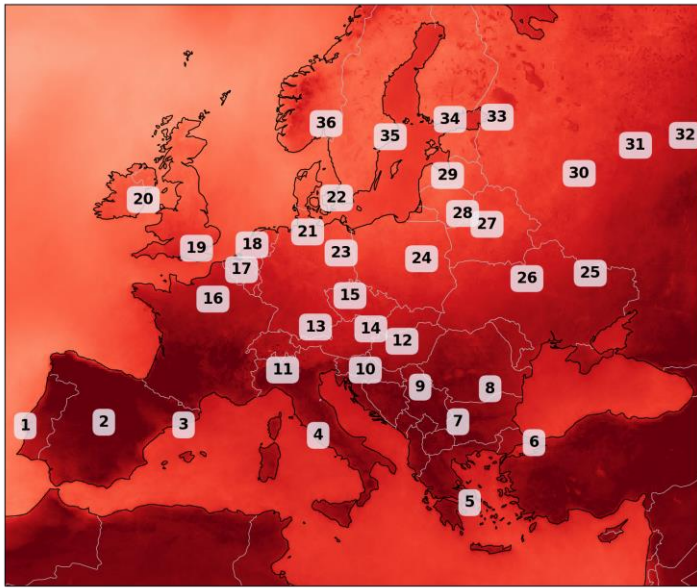
138 The analysis is based on 72 GCM–RCM model chains from the EURO-CORDEX ensemble, which covers the European  
139 domain (Jacob et al., 2013, see Supplementary Table S2 for a detailed list of models). EURO-CORDEX simulations use two  
140 different spatial resolutions, 0.11° (EUR-11, ~12.5 km) and 0.44° (EUR-44, ~50 km). We only use data from the higher-  
141 resolution EUR-11 simulations, for which typically at least one grid cell falls within the extent of each major European city  
142 (Figure 1b). For our analysis, we use daily maximum near-surface air temperature (tasmax), daily minimum near-surface air  
143 temperature (tasmin), and monthly mean near-surface air temperature (tas), employing data from historical and RCP8.5  
144 simulations for the period 1981-2100 (note that some model simulations only run until 2099 and one only until 2098). Near-  
145 surface air temperature refers to the temperature at 2 m height. For each city, we use data from the grid cell that is located  
146 closest to the centre of each city-centre. The large ensemble of 72 GCM–RCM model combinations allows for a robust  
147 estimation of future ambient heat including the model structural uncertainty, which has been shown to be relevant for  
148 quantifying the risk of urban heatwaves (Zheng et al., 2021). To test the spatial robustness of our results, we additionally  
149 consider data from a box of 3x3 grid cells around the city centres. The representation of urban areas varies considerably across  
150 RCMs (Table 1). Some RCMs represent urban areas as rock surfaces, others assume reduced vegetation and adjusted surface  
151 parameters (such as albedo and roughness) for urban areas, and one RCM even includes a sophisticated urban model.

152 We further use simulations from the CMIP5 (24 models) and CMIP6 (24 models) ensembles (using one ensemble member per  
153 model) for comparison with the EURO-CORDEX simulations (see Supplementary Tables S3 and S4 for a detailed list of the  
154 considered CMIP5 and CMIP6 models and ensemble members). We employ data from historical and RCP8.5 simulations  
155 (SSP5-8.5 in case of CMIP6), analysing daily maximum near-surface air temperature (tasmax) and monthly mean near-surface  
156 air temperature (tas) for the same period (1981-2100) as for EURO-CORDEX. Analogous to EURO-CORDEX, we use the  
157 grid cell closest to the city centre for our analysis. To evaluate how the downscaling of GCMs by RCMs affects the results, we  
158 further consider the CMIP5 model set that is used to drive the 72 EURO-CORDEX RCMs. For this purpose, we create a GCM  
159 ensemble, which we denote as “EURO-CORDEX GCM ensemble”, for which we consider each GCM member as many times  
160 as it is used as a driving GCM in the EURO-CORDEX ensemble. The EC-EARTH ensemble member r3i1p1 (used to drive

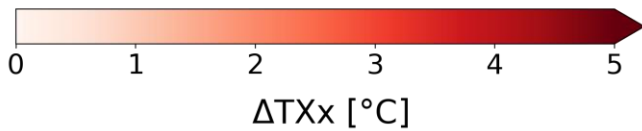
161 several EURO-CORDEX RCMs, see Supplementary Table S2) is not available via the Earth System Grid Federation (ESGF)  
162 data portals and we thus substitute it by the EC-EARTH member r1i1p1 to create the EURO-CORDEX GCM ensemble.

163 The GCMs and RCMs used in this study differ in several aspects. Most importantly, the RCMs have a much higher spatial  
164 resolution (~12.5 km) than the GCMs (~100 km), and orography and coastlines are thus represented much more accurately in  
165 RCMs. GCMs and RCMs also differ in their projections of atmospheric aerosols over the European domain, with GCMs using  
166 future scenarios with decreasing atmospheric aerosol concentrations while RCMs assume a constant atmospheric aerosol load  
167 (Boé et al., 2020; Gutiérrez et al., 2020; Nabat et al., 2020). Additionally, unlike GCMs, several RCMs do not consider plant  
168 physiological CO<sub>2</sub> effects, which might cause an underestimation of temperature extremes (Schwingshackl et al., 2019).

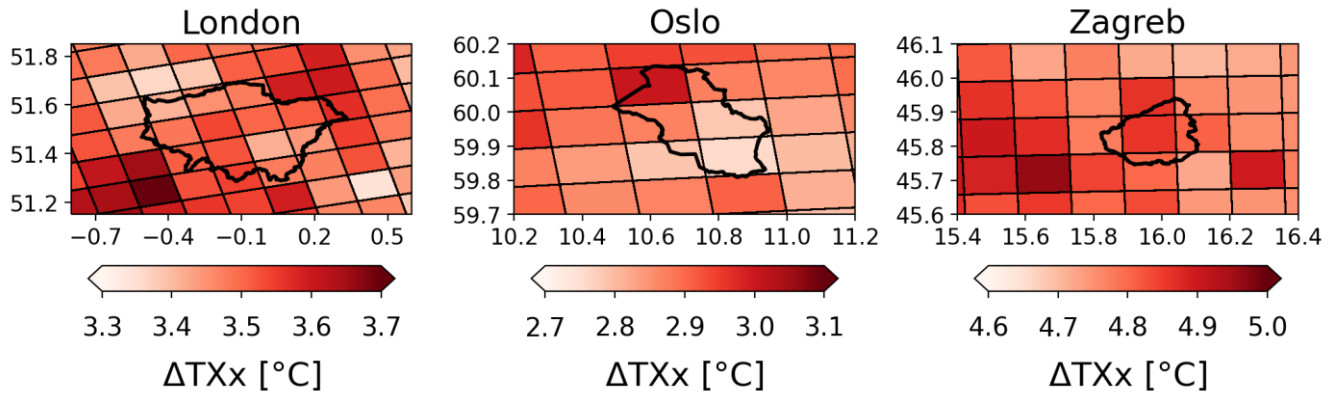
169



- |                     |                              |
|---------------------|------------------------------|
| 1: Lisbon (Lis)     | 19: London (Lon)             |
| 2: Madrid (Mad)     | 20: Dublin (Dub)             |
| 3: Barcelona (Bar)  | 21: Hamburg (Ham)            |
| 4: Rome             | 22: Copenhagen (Cop)         |
| 5: Athens (Ath)     | 23: Berlin (Ber)             |
| 6: Istanbul (Ist)   | 24: Warsaw (War)             |
| 7: Sofia (Sof)      | 25: Kharkiv (Kha)            |
| 8: Bucharest (Buc)  | 26: Kyiv                     |
| 9: Belgrade (Bel)   | 27: Minsk (Min)              |
| 10: Zagreb (Zag)    | 28: Vilnius (Vil)            |
| 11: Milan (Mil)     | 29: Riga                     |
| 12: Budapest (Bud)  | 30: Moscow (Mos)             |
| 13: Munich (Mun)    | 31: Nizhny Novgorod (Nizh)   |
| 14: Vienna (Vie)    | 32: Kazan (Kaz)              |
| 15: Prague (Pra)    | 33: Saint Petersburg (St Pe) |
| 16: Paris (Par)     | 34: Helsinki (Hel)           |
| 17: Brussels (Bru)  | 35: Stockholm (Sto)          |
| 18: Amsterdam (Ams) | 36: Oslo                     |



170  
171



172

173 **Figure 1:** Overview of the cities investigated in this study and examples of the spatial resolution of EURO-CORDEX models.  
 174 Top: Location of the cities with the background map showing the EURO-CORDEX multi-model median change of annual  
 175 maximum near-surface air temperature ( $\Delta TXx$ ) at 3 °C European warming relative to 1981-2010 (see Section 2.2).  
 176 Abbreviations in the list of cities indicate the abbreviated city names used in Figure 7. Bottom: Example of grid spacing used  
 177 by the majority of EURO-CORDEX models compared to the extent of three cities with different sizes (black polygons).

**Table 1:** Representation of urban areas in the regional climate models of the 0.11° EURO-CORDEX ensemble (EUR-11).

<u>Institute</u>	<u>Model</u>	<u>Data source</u>	<u>Representation of urban areas</u>	<u>References</u>
<u>CLMcom</u>	<u>CCLM4-8-17</u>	<u>Land-surface model TERRA</u>	<u>natural surfaces with an increased surface roughness length and a reduced vegetation cover</u>	<u>(Garbero et al., 2021; Doms et al., 2011)</u>
<u>CLMcom-ETH</u>	<u>COSMO-crCLIM-v1-1</u>	<u>Land-surface model TERRA</u>	<u>natural surfaces with an increased surface roughness length and a reduced vegetation cover</u>	<u>(Garbero et al., 2021; Doms et al., 2011)</u>
<u>CNRM</u>	<u>ALADIN53</u>	<u>ECOCLIMAP-II database</u>	<u>same as for rocks; no vegetation</u>	<u>(Daniel et al., 2018), pers. communication Samuel Somot (CNRM, 13/10/2023)</u>
<u>CNRM</u>	<u>ALADIN63</u>	<u>ECOCLIMAP-II database</u>	<u>same as for rocks; no vegetation</u>	<u>(Daniel et al., 2018; Decharme et al., 2019)</u>
<u>DMI</u>	<u>HIRHAM5</u>	<u>ECHAM5</u>	<u>adjusted constant surface parameters; vegetation not mentioned</u>	<u>(Langendijk et al., 2019; Roeckner et al., 1996, 2003)</u>
<u>MPI-CSC</u>	<u>REMO2009</u>	<u>Land Surface Parameter dataset of Hagemann (2002)</u>	<u>adjusted albedo and roughness length; no vegetation</u>	<u>(Jacob et al., 2012; Langendijk et al., 2019; Hagemann, 2002)</u>
<u>GERICS</u>	<u>REMO2015</u>	<u>Land Surface Parameter dataset of Hagemann (2002)</u>	<u>adjusted albedo and roughness length; no vegetation</u>	<u>(Jacob et al., 2012; Remedio et al., 2019)</u>
<u>ICTP</u>	<u>RegCM4-6</u>	<u>Land-surface model CLM4.5, which integrates the Community Land Model Urban (CLMU)</u>	<u>CLMU considers canyon geometry, pervious and impervious surfaces, roofs, and walls and distinguishes between four levels of urbanization; vegetation is considered as part of pervious surfaces</u>	<u>(Oleson and Feddema, 2020; Oleson et al., 2010, 2013)</u>
<u>IPSL</u>	<u>WRF381P</u>	<u>Standard canopy model from Unified Noah land-surface model (the urban canopy model implemented in WRF was not used for the EURO-CORDEX simulations)</u>	<u>bulk urban parameterization, increased surface roughness length; reduced vegetation cover</u>	<u>(Niu et al., 2011; Shen et al., 2022; Chen et al., 2011), pers. communication Linh Luu (University of Lincoln, 10/10/2023)</u>
<u>KNMI</u>	<u>RACMO22E</u>	<u>ECOCLIMAP version 1</u>	<u>no specific urban parameterization but adjusted roughness length; vegetation not mentioned</u>	<u>(van Meijgaard et al., 2008), pers. communication Erik van Meijgaard (KNMI, 8/11/2023)</u>
<u>MOHC</u>	<u>HadREM3-GA7-05</u>	<u>JULES Global Land 7.0</u>	<u>urban canopy with thermal properties of concrete; adjusted roughness length and albedo; no vegetation</u>	<u>(Best et al., 2011; Walters et al., 2019)</u>
<u>SMHI</u>	<u>RCA4</u>	<u>ECOCLIMAP version 1</u>	<u>same as for rocks (urban areas not explicitly mentioned in documentation); no vegetation</u>	<u>(Samuelsson et al., 2015), pers. communication Patrick Samuelsson (SMHI, 27/10/23)</u>

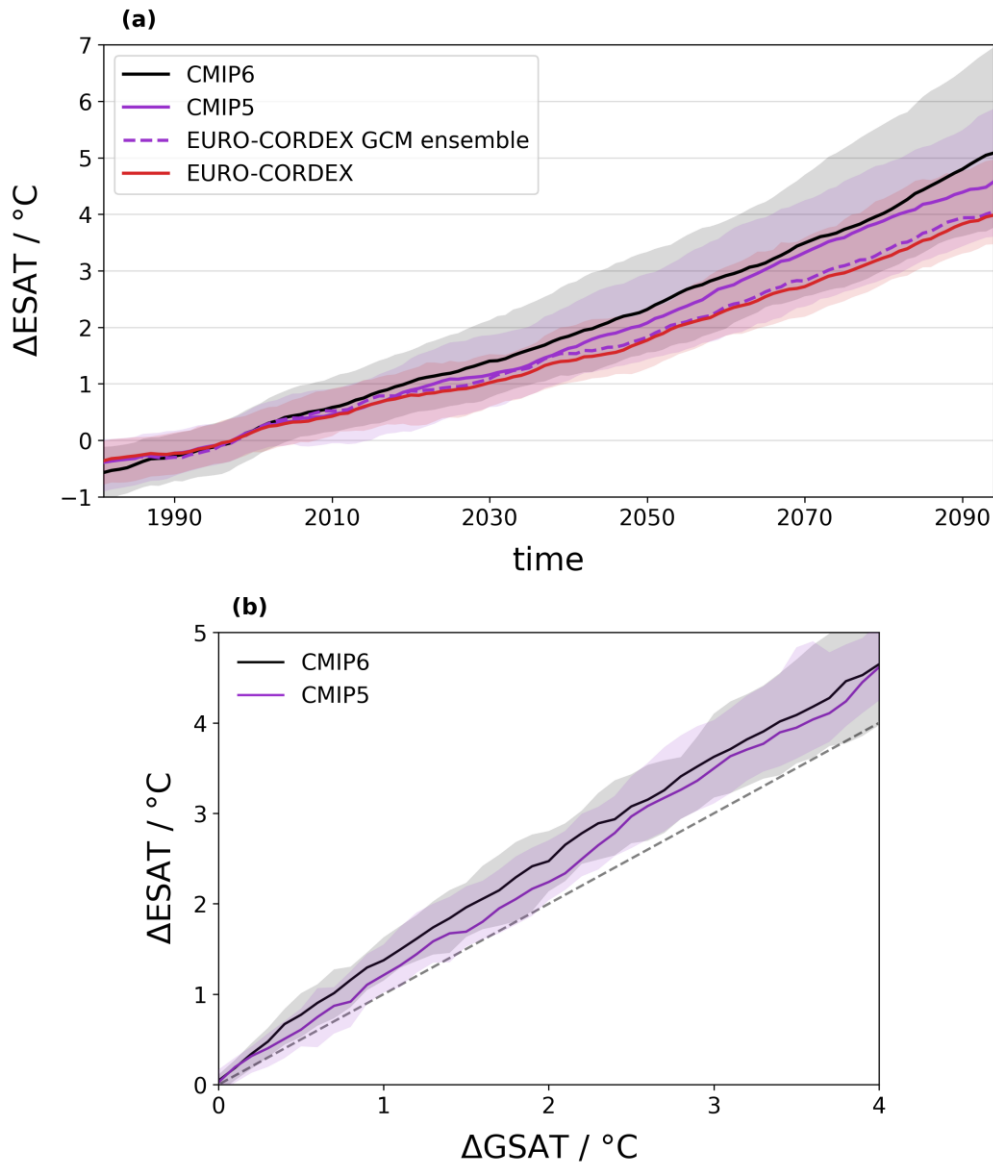


### 180 2.1.3 Reference datasets

181 We evaluate the EURO-CORDEX simulations (~~see Section 3.1~~) by comparing them against two gridded reference datasets:  
182 (~~see Section 3.1~~): 1) the E-OBS gridded meteorological dataset, which provides gridded meteorological fields interpolated  
183 from weather station data at 0.1° resolution for Europe (Cornes et al., 2018) and 2) the global reanalysis ERA5-Land, which  
184 provides land variables including 2 m air temperature at a spatial resolution of about 9 km (Muñoz-Sabater et al., 2021).  
185 Additionally, we use data from single weather stations that lie within or close to the considered cities, using data from the  
186 Global Surface Summary of the Day (GSOD; Smith et al., 2011) and from the European Climate Assessment & Development  
187 (ECA&D; Klein Tank et al., 2002; Klok and Klein Tank, 2009). We only include data from weather stations with a data record  
188 length of at least 20 years. For all datasets, the evaluation is performed using daily maximum ~~temperatures~~near-surface air  
189 temperature and daily minimum ~~temperatures~~near-surface air temperature in the period 1981-2010. For ERA5-Land, daily  
190 maximum and daily minimum near-surface air temperatures are calculated as maximum and minimum of the hourly 2 m air  
191 temperature data. The land scheme of ERA5-Land does not ~~include representations of urban areas. Hence~~specifically consider  
192 urban areas (ECMWF, 2018) and thus, specific climatic conditions in cities (such as the urban heat island effect, UHI) may  
193 not be fully represented. For cities, in which temperature data from weather stations within the city limits are assimilated in  
194 ERA5-Land or considered in E-OBS, ~~such effects~~UHI might, however, be partly included.

### 195 2.2 European mean warming

196 Regional temperatures and temperature extremes scale linearly with global mean surface air temperature (GSAT; Seneviratne  
197 et al., 2016; Wartenburger et al., 2017; Seneviratne and Hauser, 2020). Uncertainties connected to the underlying climate  
198 scenarios can thus be reduced if expressing future evolutions of regional temperatures as a function of changes in GSAT,  
199 usually calculated relative to pre-industrial (1850-1900) conditions. This approach of expressing climate change in terms of  
200 global warming levels instead of emission-driven or concentration-driven scenarios has been used by several recent studies  
201 (e.g., Schwingshackl et al., 2021; Freychet et al., 2022; Li et al., 2021) and was widely applied in the 6<sup>th</sup> Assessment Report  
202 of the Intergovernmental Panel on Climate Change (~~IPCC, 2021~~)(IPCC, 2021). While this approach works well on global  
203 scales, it cannot be applied directly to the regional climate model simulations of EURO-CORDEX, mainly due to two reasons.  
204 First, EURO-CORDEX simulations only start in 1950 (some models in 1970) and pre-industrial reference temperatures are  
205 therefore not available. We thus derive changes in mean temperatures relative to the period 1981-2010. Second, the EURO-  
206 CORDEX ensemble projects a lower rate of warming in Europe than the CMIP5 ensemble (Coppola et al., 2021). This  
207 discrepancy has been attributed to several reasons, such as differences in aerosol forcing (Boé et al., 2020; Gutiérrez et al.,  
208 2020; Nabat et al., 2020) or diverging trends in cloudiness (Bartók et al., 2017). To account for this discrepancy, we implement  
209 the scaling approach using European mean surface air temperature (ESAT) instead of GSAT based on temperature data from  
210 the EURO-CORDEX simulations. We calculate GSAT and ESAT from monthly mean temperature (tas), where ESAT is  
211 defined as the average temperature of a box spanning over Europe from 10° W to 35° E and from 30° N to 70° N.



212

213 **Figure 2:** Warming in Europe in the RCP8.5 scenario (EURO-CORDEX, CMIP5) and SSP5-8.5 scenario (CMIP6) relative to  
 214 1981-2010. (a) Change in European mean surface air temperature (ESAT) as a function of time. The dashed purple line  
 215 indicates the EURO-CORDEX GCM ensemble (see Section 2.1.2 for more details). (b) Change in ESAT as a function of  
 216 change in global mean surface air temperature (GSAT) relative to the reference period 1981-2010. Solid lines in (a) and (b)  
 217 indicate the multi-model median and shading the range from 10th to 90th percentile across models. Data in (a) are smoothed  
 218 with a 10-year window and data in (b) are interpolated in 0.1 °C steps. The dashed grey line in (b) represents the identity line.

219 Comparing the warming projections in the CMIP5, CMIP6, and EURO-CORDEX ensembles (Figure 2a) confirms that the  
220 CMIP5 and CMIP6 ensembles project a faster warming in Europe than the EURO-CORDEX ensemble. However, if  
221 considering the EURO-CORDEX GCM ensemble (see Section 2.1.2), the resulting warming projections are very similar to  
222 the projections of the EURO-CORDEX ensemble. This indicates a general agreement between the warming projections of  
223 CMIP5 and EURO-CORDEX averaged over Europe and suggests that the difference in ESAT is mainly connected to the GCM  
224 subset used to drive the EURO-CORDEX RCMs. As ESAT scales well with GSAT (Figure 2b), the warming can also be  
225 directly related to changes in GSAT.

226 For consistency, we choose to stay within the EURO-CORDEX framework and express our results as a function of ESAT  
227 instead of GSAT, based on temperature data from the EURO-CORDEX simulations. The results are shown for a European  
228 warming of 3 °C relative to 1981-2010. This corresponds to a global warming of 2.5 °C in CMIP5 (2.4 °C to 2.7 °C;  
229 interquartile range across models) and of 2.4 °C in CMIP6 (2.3 °C to 2.6 °C) relative to 1981-2010 and to a global warming  
230 of around 3.1 °C in CMIP5 (3.0 °C in CMIP6) since pre-industrial conditions (1850-1900), which lies within the range of  
231 global warming projections under current policies and actions (2.1 °C to 3.5 °C by 2100 based on the assessment by Climate  
232 Action Tracker, <https://climateactiontracker.org>, last access 09 November 2023). For each GCM-RCM model chain of EURO-  
233 CORDEX, we estimate the model-specific time when ESAT increases by 3 °C relative to 1981-2010 using a 20-year window  
234 around the first year in which the 20-year average temperature exceeds 3 °C warming. The same approach is applied to CMIP5  
235 and CMIP6 model data.

### 236 **2.3 Metrics for quantifying ambient heat**

237 Three heat metrics are used in this study to quantify how ambient heat will change in European cities under global warming.  
238 The selected metrics were applied in various studies to investigate projections of ambient heat in Europe and globally (e.g.,  
239 Casanueva et al., 2020; Lin et al., 2022; Coppola et al., 2021; Russo et al., 2015; Dosio et al., 2018). The first metric is the  
240 change in yearly maximum temperature (TXx; based on daily maximum near-surface air temperature data) between the  
241 reference period 1981-2010 and the (model-specific) time when European warming reaches 3 °C relative to 1981-2010. The  
242 change in TXx indicates how strongly extreme temperatures increase due to climate change.

243 As a second metric we calculate the number of days per year on which daily maximum ~~temperatures~~near-surface air  
244 temperature (TX) ~~exceeds~~exceeds 30 °C at the time when European warming reaches 3 °C. The threshold of 30 °C is a  
245 compromise of being high enough to be relevant for southern European countries and low enough for northern European  
246 countries. While absolute thresholds have been used in several scientific studies (e.g., Zhao et al., 2015; Schwingshackl et al.,  
247 2021; Casanueva et al., 2020), it should be kept in mind that exceedances of absolute thresholds strongly depend on local  
248 climate conditions. To test the sensitivity to the selected threshold level, we investigate how varying the threshold between 25  
249 °C and 33 °C affects the identified geographic patterns. Calculating exceedances of fixed thresholds based on climate model  
250 data usually requires bias adjustment to correct for potential model biases (Maraun, 2016). However, we do not apply bias  
251 adjustment here due to the lack of reliable reference data, as given that urban areas are not specifically represented in the

reference datasets ERA5-Land<sub>1</sub> and E-OBS<sub>2</sub>. only implicitly includes information about urban areas to the extent weather stations are present within the city limits (which does not apply to all analysed cities, see Figure 3). Consequently, the urban heat island effect might be underrepresented in these datasets. Instead, we test the effect of biasa simple adjustment by applying a simple correction method that 1) adjusts the mean of the climate model data to ERA5-Land, and 2) adjusts the mean and variability to ERA5-Land (i.e., by applying a transformation to standard score). For this purpose, the mean and standard deviation of daily maximum and daily minimum near-surface air temperatures in summer (June, July, August) isare calculated for each grid cell in a box of 5x5 grid cells around the centre of each city in the reference period 1981-2010. The resulting values are averaged over the 5x5 box and used for bias the simple adjustment method. The 5x5 box is used to represent the climate larger-scale climatological conditions within and around each city. The rationale is to reduce the statistical uncertainty by basing the adjustment on 25 grid cells instead of just one. The ERA5-Land data is bilinearly interpolated to the grid of each EURO-CORDEX model before calculating the mean and standard deviation. We use a Kolmogorov-Smirnow test to check whether the bias-adjusted heat metrics are statistically significantly different from the heat metrics calculated from the original data.

The third metric that we apply is the Heat Wave Magnitude Index daily (HWMId, Russo et al., 2015), which integrates both the length and the magnitude of a heatwave to calculate its overall strength. In the context of HWMId, heatwaves are defined as at least three consecutive days with daily maximum near-surface air temperatures above the 90th percentile of the daily maximum near-surface air temperature distribution of all days within a 31-day window in a pre-defined reference period (Russo et al., 2015). For each day in a heatwave, the HW magnitude ( $HW_M$ ) is calculated by subtracting the 25th percentile of  $TX_x$  ( $TX_{x_{25p}}$ ) in the reference period 1981-2010 from daily maximum near-surface air temperature (TX), normalised by the interquartile range of  $TX_x$  in the reference period:

$$HW_M = \begin{cases} \frac{TX - TX_{x_{25p}}}{TX_{x_{75p}} - TX_{x_{25p}}}, & \text{if } TX > TX_{x_{25p}} \\ 0, & \text{otherwise} \end{cases} \quad (1)$$

The sum over all daily HW magnitudes of a heatwave yields HWMId. By definition, HWMId takes into account the interannual temperature variability of each location. We calculate HWMId using daily maximum near-surface air temperature (denoted as HWMId-TX) for the time when European warming reaches 3 °C with 1981-2010 as the reference period. In each year, we identify the heatwave with the highest HWMId-TX and use it to calculate the 20-year average HWMId-TX.

To represent nighttime conditions, we further calculate the three different heat metrics based on daily minimum near-surface air temperature (TN), i.e., the yearly maximum of daily minimum near-surface air temperatures (TNx), the number of tropical nights (TN>20 °C), and HWMId based on daily minimum temperatures near-surface air temperature (HWMId-TN).

## 282 2.4 Statistical analysis

### 283 2.4.1 Spatial patterns of ambient heat

284 To analyse how a city's geographic location and local climate affect projections of ambient heat according to the three metrics,  
285 we estimate the contribution of different factors for explaining the spatial pattern of ambient heat across European cities. We  
286 separately analyse the spatial correlation of each heat metric with four climatological factors (summer mean daily maximum  
287 near-surface air temperature  $\overline{TX_{ref}}$  and its standard deviation  $\sigma_{TX,ref}$  in the reference period 1981-2010; change  
288 in summer mean daily maximum near-surface air temperature  $\Delta\overline{TX}$  and change in its standard deviation  $\Delta\sigma_{TX}$   
289 between reference 1981-2010 and application period (the model-specific time of 3 °C European warming) and four location  
290 factors (latitude, longitude, elevation, flag indicating whether a city is located close to the sea). Summer is defined as the  
291 months June, July, and August.

292 The explanatory variables (i.e., the climatological factors or the location factors) may be correlated, and their contributions  
293 cannot be strictly disentangled. We therefore use an approach based on semipartial correlation to quantify the average  
294 contribution of each variable to the total explained variance  $R^2$  (Schwingshackl et al., 2018). The squared semipartial  
295 correlation measures how much of the remaining unexplained variance is explained by an explanatory variable that is  
296 introduced after several others have already been considered. If explanatory variables are independent, the sum of the squared  
297 semipartial correlation coefficients yields  $R^2$ . For correlated explanatory variables, the additional contribution of an  
298 explanatory variable can be estimated by the average  $R^2$  increase of adding the variable to all regression models that contain a  
299 subset of the other explanatory variables (Azen and Budescu, 2003; Schwingshackl et al., 2018). If using the averaging method  
300 proposed by Azen and Budescu (2003), the sum of all squared semipartial correlations is equal to  $R^2$ . The variability of the  
301 squared semipartial correlation estimates is a measure for collinearities between the explanatory variables and can be used as  
302 an uncertainty estimate for the contribution of each explanatory variable. The estimated contribution of each explanatory  
303 variable to the spatial variability of each heat metric does not permit statements about causality, as it is purely based on  
304 correlation analysis. Instead, the contributions should be interpreted as a measure of the extent to which the explained variables  
305 may be influenced by the location of each city or by the climatic conditions and climate change at the location of each city.

### 306 2.4.2 Relative importance of RCMs and GCMs

307 We further quantify how much of the variability in ambient heat across the EURO-CORDEX ensemble is due to the choice of  
308 GCMs or RCM, respectively. We follow the variance decomposition method of Sunyer et al. (2015) to calculate the variance  
309 due to RCMs, due to GCMs, and due to the interaction between RCMs and GCMs. As the interaction term cannot be attributed  
310 to either GCMs or RCMs, we interpret it as uncertainty and indicate the contribution of RCMs and GCMs as a range that once  
311 includes and once excludes the contribution of the interaction term. For each heat metric, we calculate the percentage  
312 contribution of RCMs and GCMs to the total variance across all 72 RCM-GCM model chains.

## 313 3 Results

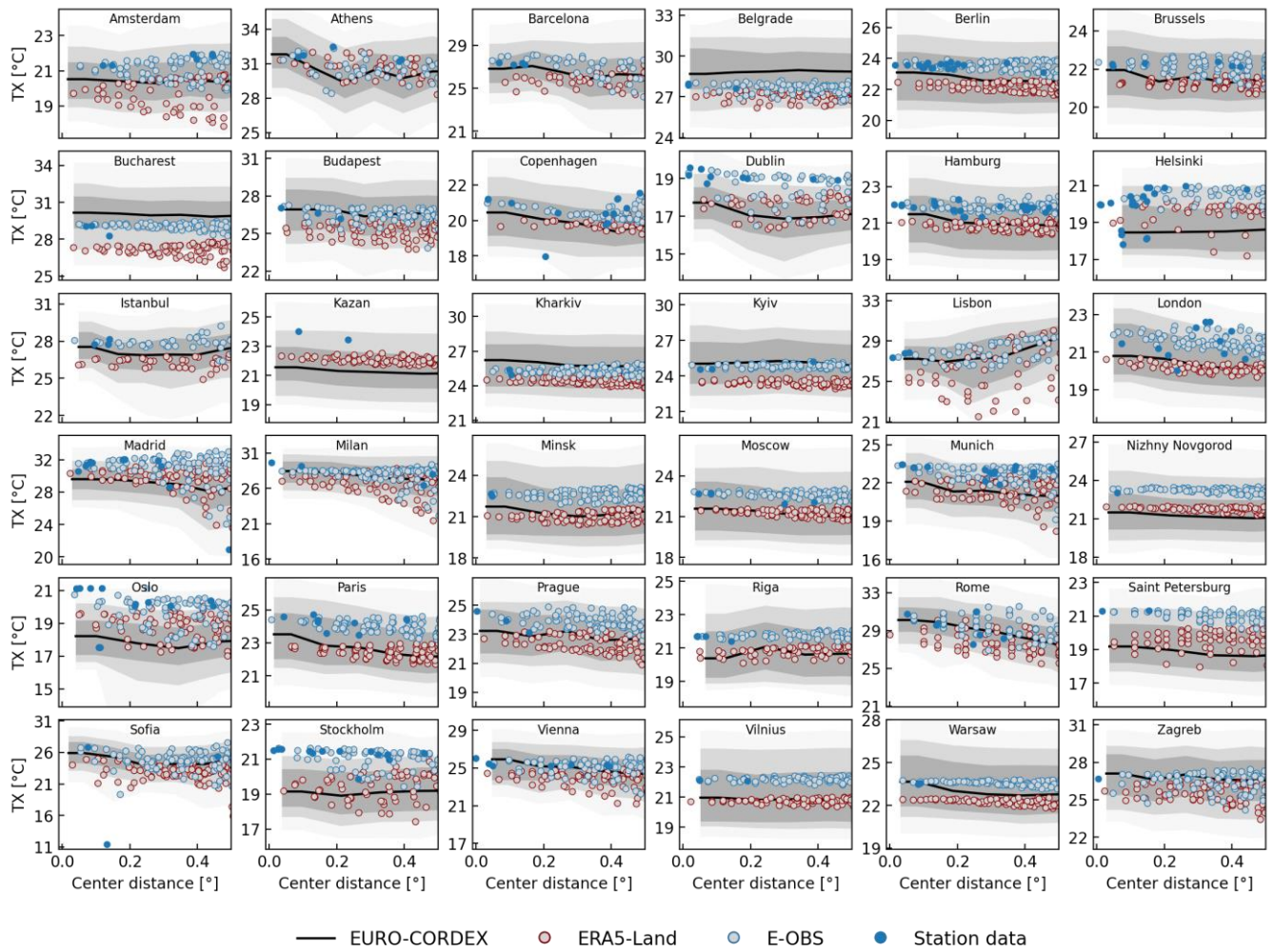
### 314 3.1 Evaluation of the EURO-CORDEX ensemble

315 To evaluate how well the EURO-CORDEX models reproduce observed temperatures in the 36 major European cities, we  
316 compare their temperature distribution to data from E-OBS, ERA5-Land, and weather stations. Figure 3 shows the distributions  
317 of summer mean daily maximum near-surface air temperatures in 1981-2010 for all cities as a function of distance from the  
318 city centre. Detailed bias distributions for all cities can be found in Supplementary Figure S1-, and a map of the multi-model  
319 median biases is shown in Supplementary Figure S2. The distribution of the EURO-CORDEX models generally matches the  
320 reference data well but is often wider than the distributions of the reference datasets (Figure 3). The EURO-CORDEX  
321 simulations reveal a cold bias in many cities lying in the northern and eastern parts of Europe (Dublin, Helsinki, Kazan, Nizhny  
322 Novgorod, Oslo, Saint Petersburg, Stockholm), ranging from -1.3 °C to -2.7 °C relative to E-OBS and from -0.3 °C to -1.2 °C  
323 relative to ERA5-Land. A warm bias – particularly relative to ERA5-Land – is found for several cities in south-eastern Europe  
324 (Belgrade, Bucharest, Kharkiv, Kyiv), ranging from +0.2 °C to +1.0 °C relative to E-OBS and from +1.7 °C to +3.2 °C relative  
325 to ERA5-Land. In general, a negative-to-positive tendency from North to South can be identified for the EURO-CORDEX  
326 biases (Supplementary Figure S2). ERA5-Land and E-OBS also show systematic differences, with daily maximum  
327 temperatures in ERA5-Land being mostly colder than E-OBS and the weather station data. Consequently, the magnitude and  
328 sign of the EURO-CORDEX biases strongly depend on the reference dataset. The multi-model median of the EURO-CORDEX  
329 ensemble has a warm bias relative to ERA5-Land (+0.5 °C on average across cities) and a cold bias relative to E-OBS (-0.8  
330 °C on average), which is consistent with the findings of Vautard et al. (2021).

331 The distributions of daily minimum near-surface air temperatures in the EURO-CORDEX models also generally match the  
332 reference datasets (Supplementary Figure S2), ~~but in several cities biases are more pronounced than for maximum~~  
333 ~~temperatures.S3), although the spatial patterns differ from the bias patterns of maximum temperatures (Supplementary Figure~~  
334 ~~S2). Biases are highest in northern, eastern, and southern European cities, while they are lowest in central European cities~~. The  
335 EURO-CORDEX ensemble has a cold bias relative to E-OBS (-0.6 °C on average; most pronounced in Saint Petersburg,  
336 Nizhny Novgorod, Copenhagen, Lisbon, Madrid) and to ERA5-Land (-0.8 °C on average; most pronounced in Kazan, Helsinki,  
337 Istanbul, Riga, Stockholm). In contrast to the lower daily maximum temperature values in ERA5-Land, daily minimum  
338 temperatures in ERA5-Land are warmer than E-OBS in several of the investigated cities.

339 In ~~several~~some cities, temperatures ~~change depending on~~vary as a function of the distance from the city centre (Figure 3,  
340 Supplementary Figure ~~S2~~S3). E-OBS shows higher temperatures close to the city centre in Budapest, Prague, and Vienna,  
341 while for EURO-CORDEX this is the case in Athens, Brussels, Dublin, Minsk, Munich, Paris, Rome, and Vienna. Yet, these  
342 temperature gradients are not necessarily due to UHI but could also be caused by other factors, such as gradients in elevation.  
343 For E-OBS and the weather station data, the scarce station density close to the city centres as well as the standard conditions  
344 for meteorological measurements (i.e., measurements are taken over grasslands) might be reasons for the lack of pronounced  
345 UHI effects. For the other datasets, this might be due to the missing representation of urban areas in the land surface schemes

346 of ERA5-Land and ~~in many~~the predominantly rather simple representation of urban areas in the EURO-CORDEX models-  
347 (Table 1).



348

349

350

351

352

353

354

**Figure 3:** Distribution of daily maximum near-surface air temperature (TX) in summer for the investigated European cities as function of distance to the city centre. The plot shows summer (June, July, August) average TX over the period 1981-2010 for EURO-CORDEX (black line and grey shading), ERA5-Land (red-edged grey dots), E-OBS (blue-edged grey dots), and station data (filled blue dots). The black line for EURO-CORDEX denotes the multi-model median, dark grey shading the interquartile range across models, and light (very light) grey shading the range from 10th (1st) to 90th (99th) percentile. Only temperatures on land are included (sea areas are masked).



### 355 3.2 Projections of ambient heat for major European cities

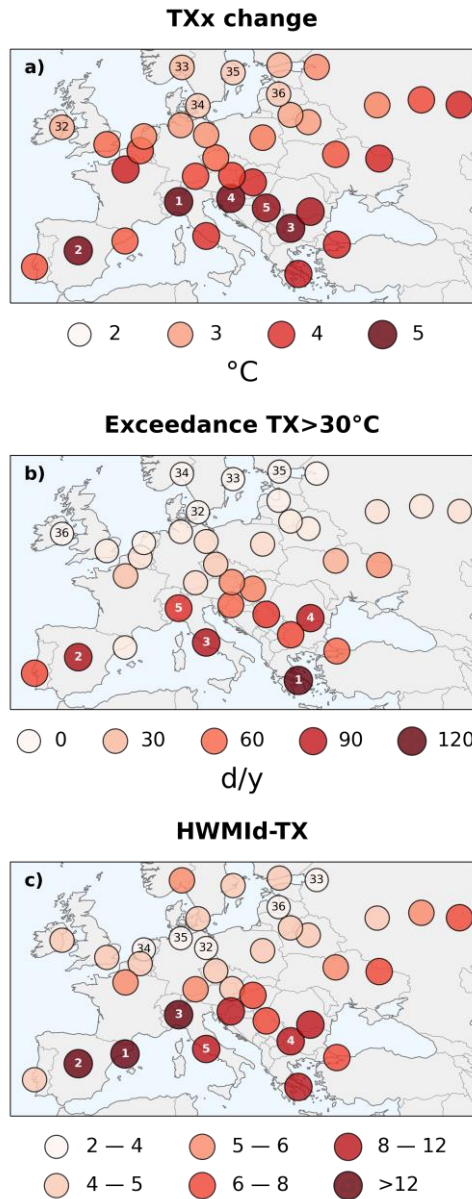
356 The EURO-CORDEX projections for major European cities show increasing ambient heat under 3 °C European warming with  
357 distinct geographical patterns for the three different metrics (Figure 4). Increases in TXx are largest in southern Europe,  
358 followed by western and eastern Europe, and ~~lower towards~~lowest in northern Europe. The top five cities in terms of TXx  
359 increase (Milan, Madrid, Sofia, Zagreb, Belgrade; numbered from 1 to 5 in Figure 4) are all located in southern Europe but  
360 none of them is located ~~directly~~ close to the sea. Cities in southern Europe located at or close to the sea (e.g., Lisbon, Barcelona,  
361 Rome, Athens, Istanbul) also show substantial TXx increase, yet weaker than the cities situated more inland.

362 The yearly number of days on which TX exceeds 30 °C shows a clear south-~~to~~-north gradient, with values being highest in  
363 Athens, Madrid, Rome, Bucharest, and Milan (numbered 1 to 5). These cities exceed 30 °C on more than 80 d/y, while the  
364 five cities with lowest exceedance rates (all lying in northern Europe; numbered 32 to 36) experience on average less than 2  
365 d/y above 30 °C. Additionally, local climate conditions can play an important role as well, for example in the case of Barcelona,  
366 Istanbul, and Sofia, which have lower exceedance rates than the surrounding cities. Varying the threshold level between 25 °C  
367 and 33 °C considerably changes the number of yearly exceedance days, but the geographical distribution is not altered much  
368 (Supplementary Figure [S3S4](#)).

369 HWMI<sub>d</sub>-TX is largest in southern European cities, followed by eastern European cities, with values being highest in Barcelona,  
370 Madrid, Milan, Sofia, and Rome (numbered 1 to 5). In contrast to the other two metrics, cities located in northern Europe also  
371 show high HWMI<sub>d</sub>-TX values (e.g., Oslo, Copenhagen, Stockholm, Helsinki), while lowest HWMI<sub>d</sub>-TX values are projected  
372 in an arc spanning from the Netherlands over northern Germany towards the Baltic states.

373 ~~Several~~In several cities-, all considered heat metrics show high levels of ambient heat ~~for all investigated heat metrics under 3~~  
374 °C European warming (e.g., Athens, Belgrade, Bucharest, Madrid, Milan, Sofia, Zagreb), ~~while~~. ~~For~~ other cities ~~reveal a~~  
375 ~~strong dependency, however, the ambient heat levels differ substantially depending~~ on the metric under consideration.  
376 Barcelona, for example, ranks number one in terms of HWMI<sub>d</sub>-TX, but exceeds 30 °C only rarely. Lisbon has substantial  
377 increases in TXx and temperatures often exceed 30 °C, but HWMI<sub>d</sub>-TX is rather low. Kazan has substantial increases in TXx  
378 and high HWMI<sub>d</sub>-TX values, but TX exceedances above 30 °C are relatively low. Oslo ranks among the cities with weakest  
379 changes in TXx and with lowest TX exceedances above 30 °C, but with high HWMI<sub>d</sub>-TX values. ~~Considering only one~~These  
380 discrepancies may be due to several reasons. For instance, cities with comparatively cooler climate may see large increases in  
381 TXx and high HWMI<sub>d</sub>-TX values without having substantial exceedances above 30 °C. Cities with high climatological  
382 variability in TXx may have comparatively low HWMI<sub>d</sub>-TX values despite large increases in TXx and, vice versa, relatively  
383 low increases in TXx might result in high HWMI<sub>d</sub>-TX values in case of low climatological variability in TXx. Considering  
384 only one heat metric might thus lead to unbalanced conclusions about projections of ambient heat for urban areas, potentially  
385 underestimating future risks from heat stress.

386



387

388

389

390

391

392

393

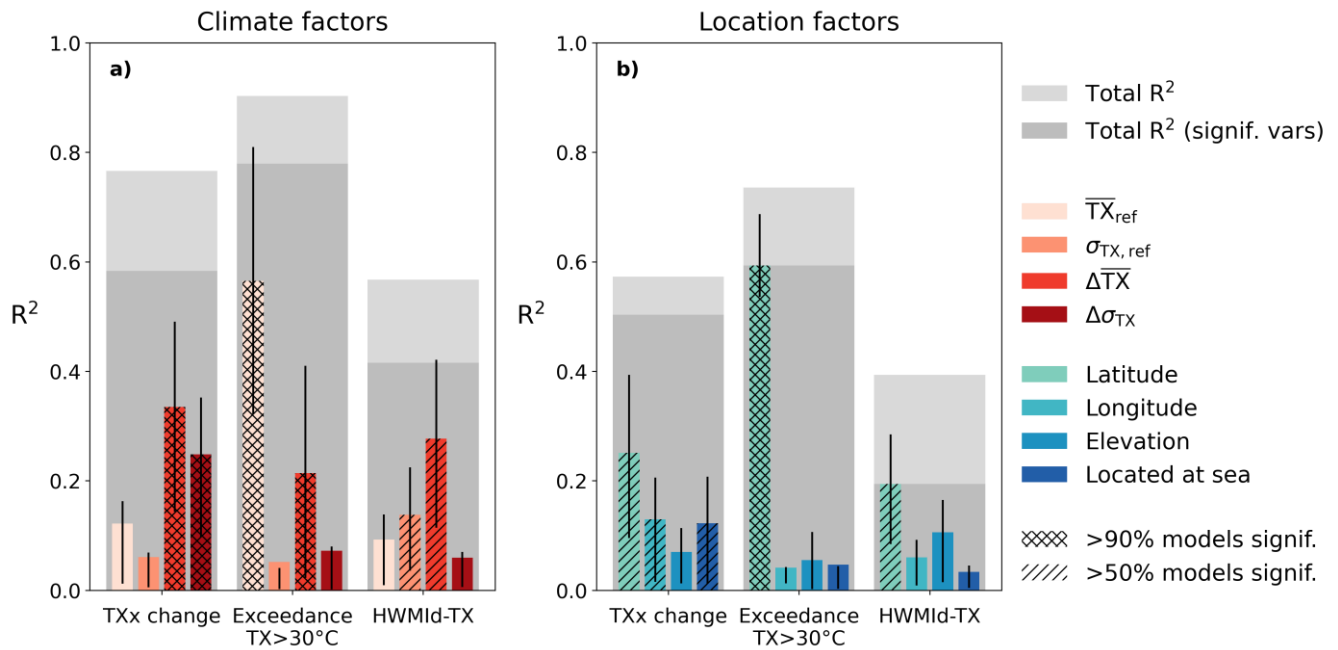
**Figure 4:** Projections of ambient heat at 3 °C European warming according to three different heat metrics for 36 major European cities as simulated by the EURO-CORDEX ensemble. a) Change in yearly maximum near-surface air temperature (TXx) between 1981-2010 and 3 °C European warming, b) TX exceedances above 30 °C at 3 °C European warming, and c) Heat Wave Magnitude Index daily based on TX (HWMid-TX) at 3 °C European warming. The values indicate the multi-model median of the EURO-CORDEX ensemble. Numbers in the circles from 1 to 5 (32 to 36) indicate the five cities with highest (lowest) ambient heat according to each metric.

### 394 3.3 Identifying factors influencing the spatial patterns of ambient heat across cities

395 To better understand the ~~projected~~ spatial patterns of ambient heat projected by the ~~three different~~ heat metrics, we estimate  
396 how much of the spatial variance is explained 1) by different climate factors, representing each city's temperature climatology  
397 as well as its projected changes, and 2) by different location factors (Figure 5). ~~Generally, the considered climate factors ( $\overline{TX}_{ref}$ ,  
398  $\sigma_{TX,ref}$ ,  $\Delta\overline{TX}$ , and  $\Delta\sigma_{TX}$ ; see Section 2.4.1 for methodological details). Generally, the considered climate factors ( $\overline{TX}_{ref}$ ,  $\sigma_{TX,ref}$ ,  
399  $\Delta\overline{TX}$ , and  $\Delta\sigma_{TX}$ ; see Section 2.4.1 for their definition) explain more of the spatial patterns than the location factors (latitude,  
400 longitude, elevation, location close to sea). Regarding climate factors (Figure 5a), the spatial pattern of TXx change is mostly  
401 influenced by the climate factors  $\Delta\overline{TX}$  and  $\Delta\sigma_{TX}$ , while climate conditions in the reference period do not contribute  
402 significantly. For TX exceedances above 30 °C, the maximum temperature in the reference period contributes by far the most,  
403 followed by  $\Delta\overline{TX}$ . For HWMId-TX, the strongest contributions stem from  $\Delta\overline{TX}$  and  $\sigma_{TX,ref}$ . Regarding location factors (Figure  
404 5b), latitude, longitude, and whether a city is located close to the sea partly explain the spatial pattern of TXx change, albeit  
405 with rather low model agreement. For the TX exceedances above 30 °C, latitude plays the dominant role, while the  
406 contributions of all other factors remain negligible. For HWMId-TX, the explanatory power of all location factors remains  
407 low, with latitude being the only factor that explains some of the signal.~~

408 Across the three metrics, most of the spatial variability can be explained for the TX exceedances above 30 °C ( $R^2=0.78$  for  
409 climate and  $R^2=0.59$  for location factors; considering only variables with significant contribution in at least 50% of the EURO-  
410 CORDEX models), followed by TXx change ( $R^2=0.58$  for climate and  $R^2=0.50$  for location factors), while the explained  
411 variance of the spatial patterns of HWMId remains rather low ( $R^2=0.42$  for climate and  $R^2=0.19$  for location factors). The  
412 contribution of the single climate factors depends strongly on the selected metric, whereas for location factors only latitude  
413 plays a major role. All other location factors – despite being statistically significant in some cases – only contribute little to  
414 the total variance explained. The high uncertainty for the contribution of some explanatory variables (e.g.,  $\Delta\overline{TX}$  and  $\Delta\sigma_{TX}$  for  
415 TXx change,  $\overline{TX}_{ref}$  and  $\Delta\overline{TX}$  for TX exceedances above 30 °C) points to collinearities between these explanatory variables,  
416 which can, however, not be disentangled based on correlation analysis.

417



418

419

420

421

422

423

424

425

426

427

428

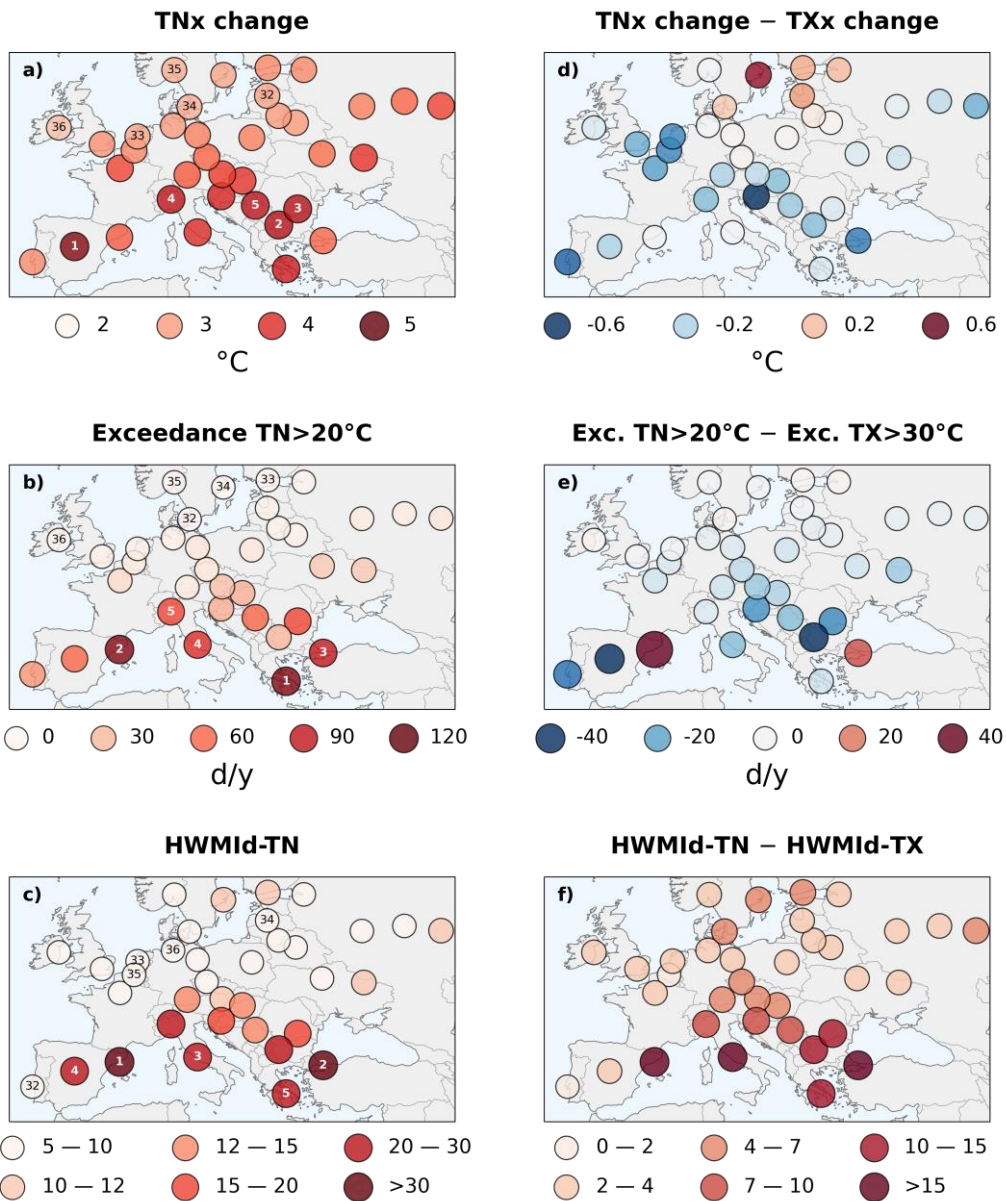
429

430

**Figure 5:** Contribution of different explanatory variables to the explained variance ( $R^2$ ) of the spatial patterns of ambient heat across European cities in the EURO-CORDEX ensemble. Explanatory variables are divided into a) climate factors (summer mean daily maximum near-surface air temperature  $\overline{TX}_{ref}$  and its standard deviation  $\sigma_{TX,ref}$  in the reference period; change in summer mean daily maximum near-surface air temperature  $\Delta\overline{TX}$  and its standard deviation  $\Delta\sigma_{TX}$  between the reference period 1981-2010 and 3 °C European warming) and b) location factors. Coloured bars denote the median estimate for each factor, black whiskers denote the uncertainty indicated as interquartile range (calculated from the pooled data of all 72 EURO-CORDEX models and eight regression models). Hatching with lines (crosses) indicates whether at least 50% (90%) of the EURO-CODEX models indicate statistically significant contribution of the respective explanatory variable (Student's t-test,  $p < 0.05$ ). Background bars coloured in light grey indicate total  $R^2$  considering all explanatory variables, background bars in dark grey indicate total  $R^2$  if considering only explanatory variables that are statistically significant in at least 50% of the EURO-CORDEX models (Student's t-test,  $p < 0.05$ ). The contribution of each climate/location factor is estimated by semipartial correlation (see Section 2.4.1).

### 3.4 Comparing projections of ambient heat during daytime and nighttime

The results presented so far are based on daily maximum temperature and are thus mostly indicative for daytime conditions. We additionally consider daily minimum temperature (TN) to investigate projections of ambient heat during nighttime, which play an important role for human health as well, since elevated nighttime temperatures can reduce people's capacity to recover and thus weaken their physical conditions (Royé et al., 2021; Thompson et al., 2022). The geographical patterns of the TN-based heat metrics are generally similar to the TX-based patterns (Figure 6) with highest levels of ambient heat in southern European cities. Yet, several distinct differences are evident. The TNx increase is generally smaller than the TXx increase, except for cities located at the Baltic Sea, which exhibit a stronger increase in TNx than TXx. Days with TN>20 °C ("tropical nights") are rarer than days with TX>30 °C, except for Barcelona and Istanbul, both of which having substantially more days with TN>20 °C than TX>30 °C (note that no bias adjustment was applied neither for TN>20 °C nor for TX>30 °C; bias-adjusting the mean of the TN distribution based on ERA5-land data even increases the days with TN>20 °C in Barcelona and Istanbul; not shown). In northern Europe, days with TN>20 °C or TX>30 °C both occur very rarely, and differences are thus negligible. Varying the TN threshold level between 15 °C and 23 °C considerably changes the number of yearly exceedance days, but the geographical distribution is not altered much (not shown). HWMId-TN shows much higher values than HWMId-TX, particularly in southern European cities but also in central European cities and in several cities located at the Baltic Sea. Differences between HWMId-TN and HWMId-TX are particularly large in Istanbul, Barcelona, and Rome. The higher HWMId-TN values suggest that nighttime heatwaves will become more severe than daytime heatwaves in the investigated cities as compared to the typical nighttime and daytime climate conditions of the recent past (1981-2010).



450

451

452

453

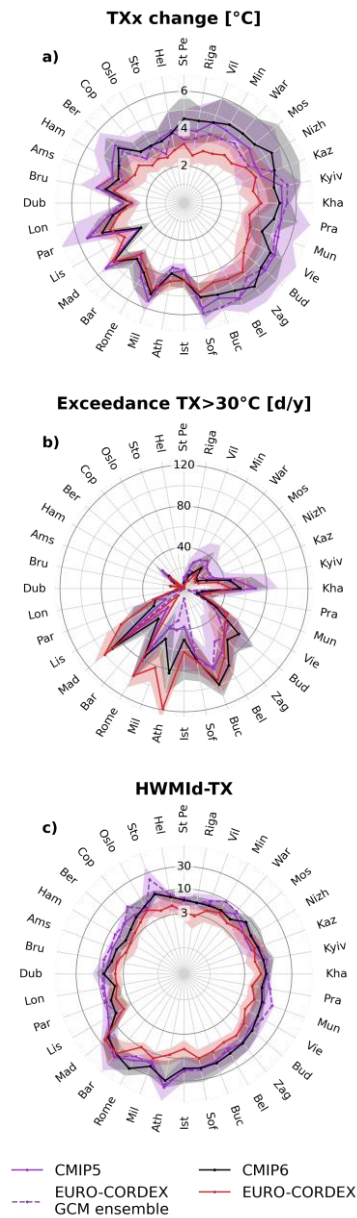
**Figure 6:** As in Figure 4 but for daily minimum near-surface air temperature (TN) in panels (a) - (c). Panels (d) - (f) show the difference between ambient heat estimates based on TN and based on daily maximum near-surface air temperature (TX). Note that the scale for HWMid-TN differs from the HWMid-TX scale in Figure 4.

### 454 3.5 EURO-CORDEX projections of ambient heat in comparison to CMIP5 and CMIP6 projections

455 We further compare the projections of ambient heat by the EURO-CORDEX, CMIP5, and CMIP6 ensembles for the 36  
456 European cities (Figure 7). The general patterns of CMIP5 and CMIP6 reflect the results of Figure 4, showing a strong TXx  
457 increase in south-eastern and eastern European cities, high TX exceedance rates of 30 °C in southern and some eastern  
458 European cities, and high HWMId-TX values in southern and some northern European cities (note the logarithmic axis for the  
459 latter). In terms of TXx change, the CMIP5 and CMIP6 ensembles generally project a stronger increase in ambient heat than  
460 the EURO-CORDEX models, particularly in south-eastern, eastern, and north-eastern European cities, while, for Lisbon,  
461 Athens, and Istanbul, the EURO-CORDEX ensemble projects stronger TXx increases. Regarding TX exceedances above 30  
462 °C, the EURO-CORDEX ensemble projects much higher exceedance rates than the CMIP5 and CMIP6 ensembles in southern  
463 European cities (e.g., Lisbon, Milan, Athens, Istanbul), whereas the CMIP5 and CMIP6 ensembles show larger exceedance  
464 rates in north-eastern European cities and in Barcelona. The CMIP5 and CMIP6 ensembles project higher HWMId-TX values  
465 in almost all cities except Madrid, Nizhny Novgorod, and Kazan. Differences in HWMId-TX between the CMIP5 and CMIP6  
466 and EURO-CORDEX ensembles are particularly pronounced in Stockholm, Rome, Athens, and Istanbul. The projected  
467 geographical patterns of ambient heat from the CMIP5 and CMIP6 ensembles are generally similar; notable differences are  
468 only found for TX exceedances above 30 °C, where CMIP6 has substantially higher values in southern European cities  
469 ~~and~~ whereas CMIP5 shows more exceedances in northern European cities.

470 To investigate the effect of dynamical downscaling by RCMs, we additionally consider the projections of ambient heat by the  
471 EURO-CORDEX GCM ensemble (dashed purple line in Figure 7; see Section 2.1.2 for its definition). The EURO-CORDEX  
472 GCM ensemble resembles more closely the results of the CMIP5 ensemble than of the EURO-CORDEX ensemble, except for  
473 some cities (e.g., Amsterdam, Copenhagen, Stockholm, Saint Petersburg, Nizhny Novgorod for TXx changes; Rome for TX  
474 exceedances above 30 °C; Lisbon for HWMId-TX). In combination with the fact that the EURO-CORDEX GCM ensemble  
475 ~~shows~~ show very similar ESAT trends to the EURO-CORDEX RCM ensemble (Figure 2a), this indicates that differences in  
476 projections of ambient heat between the EURO-CORDEX and CMIP5 ensembles are mostly connected to the dynamical  
477 downscaling by RCMs. For cities located close to mountains (e.g., Athens) or close to the sea (e.g., Lisbon, Barcelona,  
478 Stockholm), the higher spatial resolution of RCMs should thus deliver more accurate estimates than the more coarsely resolved  
479 GCMs. This is reflected in the large differences between CMIP5 and EURO-CORDEX estimates for several cities, particularly  
480 for TX exceedances above 30 °C and for HWMId-TX.

481



482

483

484

485

486

487

488

489

**Figure 7:** Projections of ambient heat in European cities for EURO-CORDEX, CMIP5, CMIP6, and the EURO-CORDEX GCM ensemble. Cities are arranged according to their geographical location, i.e., northern European cities at the top, eastern European cities on the right, southern European cities at the bottom, and western European cities on the left. a) Change in yearly maximum near-surface air temperature (TXx) between 1981-2010 and 3 °C European warming, b) TX exceedances above 30 °C at 3 °C European warming, c) Heat Wave Magnitude Index daily based on TX (HWMId-TX) at 3 °C European warming. Note the logarithmic axis for the HWMId-TX panel. Lines indicate the multi-model median and shading the interquartile range across models.



### 490 3.6 Uncertainty of ambient heat projections

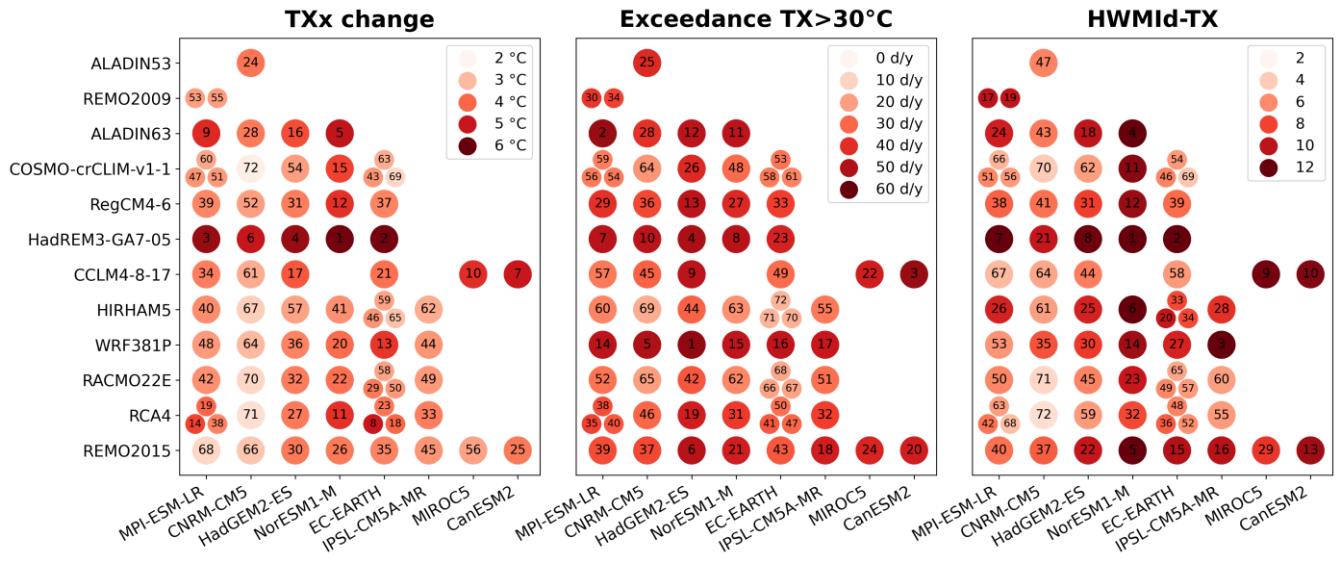
491 To evaluate the robustness of our results, we estimate how strongly the estimates of ambient heat vary across the EURO-  
492 CORDEX models and how much they change in space, that is, within a box of 3x3 grid cells around the grid box located  
493 closest to the city centres. The large ensemble of 72 GCM-RCM combinations enables a thorough assessment of the model  
494 uncertainty, which we quantify here as the interquartile range (IQR) across models (Figure 7). Uncertainties of TXx change  
495 lie between 1 °C and 2 °C in almost all cities, with uncertainties being lowest in southern European cities (where uncertainties  
496 are ~1 °C). For TX exceedances above 30 °C, we calculate relative uncertainties (IQR divided by multi-model median; not  
497 shown) to reflect the large variability of exceedance rates across cities. The relative uncertainties of TX exceedances above 30  
498 °C are lowest in southern European cities (between 20% and 60%) except for Barcelona, where the relative uncertainty is  
499 larger than 300% (and the distribution is skewed towards higher values). In contrast to the other metrics, the uncertainties of  
500 HWMI<sub>d</sub>-TX are higher in southern European cities (uncertainties lying between 4 and 8) than in northern European cities  
501 (uncertainties lying between 2 and 6), with uncertainties being highest in Barcelona (IQR = 32) followed by Madrid (IQR =  
502 13).

503 To quantify the spatial variability of ambient heat, we calculate the heat metrics ~~are calculated~~ individually for each grid cell  
504 in a box of 3x3 grid cells around the city centres. The spatial variability is quantified by how much ambient heat varies  
505 ~~over~~within the 3x3 grid cells (Supplementary Figure S4S5). In the large majority of cities, the TXx change estimates remain  
506 very similar if using the 3x3 box, indicating that the estimated trends in TXx do not change much within the grid cells  
507 surrounding the city centres. Lisbon, Barcelona, Athens, Helsinki, and Istanbul are the cities with the largest spatial  
508 variability in TXx changes. Regarding TX exceedances above 30 °C, the largest variabilities are found in Lisbon, Barcelona,  
509 Athens, Istanbul, Rome, and Sofia. HWMI<sub>d</sub>-TX values show very large spatial variability in Barcelona and Helsinki, and  
510 pronounced variability in Istanbul, Copenhagen, Athens, and Dublin. If only considering grid cells with land fractions larger  
511 than 25%, 50%, or 75%, the variability decreases substantially in almost all ~~the~~ cities with large spatial variability in heat  
512 metrics. This suggests that ambient heat strongly differs between land and sea areas, particularly for HWMI<sub>d</sub>-TX and for TX  
513 exceedances above 30 °C. For HWMI<sub>d</sub>-TX this might be due to the higher TXx variability over land areas than over the sea  
514 in the reference period 1981-2010 (Supplementary Figure S5S6), resulting in much larger HWMI<sub>d</sub>-TX values over sea than  
515 over land. Consequently, cities located close to the sea might be affected by this stark land-sea contrast, particularly if their  
516 climate is strongly influenced by the sea.

517 We further test how TX exceedances above 30 °C in the grid cell closest to the centre of each city change if applying a simple  
518 ~~bias~~-adjustment method that 1) adjusts the mean of each EURO-CORDEX model to the mean of the ERA5-Land data and 2)  
519 adjusts both the mean and the standard deviation (Supplementary Figure S6S7, see also Section 2.3 for methodological details).  
520 The most striking effect of ~~bias~~-adjusting the data is a reduced uncertainty of the projected TX exceedances above 30 °C.  
521 Moreover, the ~~bias~~-adjusted exceedance rates are statistically significantly lower in 13 cities and higher in 2 cities if only the  
522 mean is adjusted (Kolmogorov-Smirnow test,  $p < 0.05$ ); and lower in 15 cities and higher in 6 cities if both mean and standard

523 deviation are adjusted. In the remaining cities, the differences are not statistically significant. The effects of ~~bias~~the simple  
524 adjustment method are largest in Lisbon, Rome, Sofia, and Bucharest with substantially lower exceedance rates in case of ~~bias~~  
525 adjustment. Adjusting only the mean or adjusting both mean and standard deviation generally yields similar results (differences  
526 are largest in Istanbul and Lisbon) with the latter method tending to yield lower exceedance rates.

527 The rather complete matrix of RCM-GCM combinations enables us to quantify how much of the variability in ambient heat  
528 across the EURO-CORDEX models is due to the choice of GCMs or RCMs (Figure 8, see section 2.4.2 for methodological  
529 details). The variability across all RCM-GCM combinations is mostly due to RCMs (60% to 75% for TXx change, 60% to  
530 70% for TX exceedances above 30 °C, and 50% to 65% for HWMId-TX), highlighting that the downscaling by RCMs plays  
531 a crucial role for the ambient heat estimates in urban areas. Additionally, several patterns can be identified for certain RCMs  
532 and GCMs, which indicates that the choice of RCMs and GCMs is also important. Among RCMs, projections of ambient heat  
533 in terms of TXx change and HWMId-TX are highest for HadREM3-GA7-05, and in terms of TX exceedances above 30 °C  
534 values are highest for WRF381P, HadREM3-GA7-05, and ALADIN63. Comparatively low increases in ambient heat are  
535 projected by the RCMs HIRHAM5, RACMO22E, and COSMO-crCLIM-v1-1. Differences between GCMs are less  
536 pronounced. Projections of ambient heat are highest for NorESM1-M and CanESM2 in terms of TXx change, for CanESM2,  
537 HadGEM2-ES, and MIROC5 in terms of TX exceedances above 30 °C, and for NorESM1-M, CanESM2, and MIROC5 in  
538 terms of HWMId-TX. It should be noted though that the results for CanESM2 and MIROC5 might be less robust as each of  
539 them is only used twice as driving GCM. Comparatively low increases in ambient heat are projected by CNRM-CM5 and  
540 IPSL-CM5A-MR for TXx change, by EC-EARTH and CNRM-CM5 for TX exceedances above 30 °C, and by CNRM-CM5  
541 and MPI-ESM-LR for HWMId-TX.



544

545

546

547

548

549

550

**Figure 8:** GCM-RCM matrix of EURO-CORDEX models for the change in yearly maximum near-surface air temperature (TXx) between 1981-2010 and 3 °C European warming, b) TX exceedances above 30 °C at 3 °C European warming, and c) Heat Wave Magnitude Index daily based on TX (HWMid-TX) at 3 °C European warming. Each circle indicates the average value across all investigated cities for each individual EURO-CORDEX model. Numbers in the circle indicate the ranking of models from 1 (highest ambient heat) to 72 (lowest ambient heat). Multiple ensemble members for a GCM-RCM combination are indicated as smaller circles.

## 551 4 Discussion

### 552 4.1 Interpretation and implications of results

553 All three analysed heat metrics show strong increases in ambient heat in southern European cities at 3 °C European warming.  
554 Substantial increases in ambient heat are also evident in other European regions; yet, the spatial patterns strongly depend on  
555 the metric under consideration. TXx increases considerably in western and eastern Europe, TX exceedances above 30 °C show  
556 a clear south-to-north gradient with almost no exceedances in northern European cities, and HWMId-TX yields comparatively  
557 high values in eastern and northern European cities. This has implications for the estimation of future heat stress, as the  
558 projected outcomes can vary strongly depending on the considered metric. For instance, regions in northern Europe that are  
559 usually not considered as very prone to heat stress show relatively high values of HWMId-TX. Since health impacts do not  
560 only depend on universal physiological limits but also on the climate conditions people are used to (Petkova et al., 2014;  
561 Åström et al., 2013), metrics considering the climatology of a region (such as HWMId-TX) can give important insights into  
562 the risk of future heat stress that might otherwise be missed. This also concerns nighttime conditions, as HWMId-TN is even  
563 higher than HWMId-TX (Figure 6).

564 The identified spatial patterns broadly agree with results of other studies, showing an increase in heatwave risk in southern  
565 Europe along with substantial increases in coastal regions in northern Europe (Guerreiro et al., 2018; Smid et al., 2019; Lin et  
566 al., 2022) – as we find for HWMId-TX – and a clear south-to-north gradient in exceedances of WBGT>28 °C (Casanueva et  
567 al., 2020) – consistent with the patterns of TX exceedances above 30 °C. Guerreiro et al. (2018) found that temperatures during  
568 heatwaves increase strongest in central Europe, while the TXx increases estimated in our study are highest in southern  
569 European cities. This discrepancy between the findings of Guerreiro et al. (2018) and our results could, on the one hand, be  
570 related to the fact that TXx does not directly reflect temperatures during heatwaves. On the other hand, it could also be due to  
571 the more pronounced increase of extreme temperatures in central Europe in CMIP5 compared to EURO-CORDEX  
572 (Supplementary Figure S7)–S8). Supplementary Figure S8 also shows that the EURO-CORDEX models project an amplified  
573 warming of the Baltic Sea compared to the surrounding land areas, which is likely the reason for the high values of HWMId-  
574 TX in northern European coastal cities.

575 In many of the investigated cities, CMIP5 and CMIP6 project higher increases in TXx and larger HWMId-TX values than  
576 EURO-CORDEX. This is likely caused by discrepancies in external forcing data and differences in process implementation  
577 (see Section 2.1.2). Specifically, the CMIP5 and CMIP6 simulations are based on future scenarios with decreasing atmospheric  
578 aerosol concentrations over the European domain, while the EURO-CORDEX simulations assume a constant atmospheric  
579 aerosol load (Boé et al., 2020). The RCMs of EURO-CORDEX may thus underestimate future warming in Europe as they do  
580 not consider the amplified warming from the additional solar radiation reaching and heating the Earth’s surface in Europe  
581 because of the decreasing aerosol concentrations. In addition, unlike CMIP5 and CMIP6 GCMs, several RCMs do not consider  
582 plant physiological effects (Schwingshackl et al., 2019). The closing of plant stomata due to higher CO<sub>2</sub> concentrations and  
583 the associated decrease in latent and increase in sensible heat fluxes, which lead to enhanced extreme temperatures, are thus

584 not fully captured by RCMs. These differences between GCMs and RCMs suggest that RCMs likely underestimate future  
585 levels of ambient heat in European cities. Yet, for several southern European cities the EURO-CORDEX models project  
586 considerably more days exceeding 30 °C than CMIP5 and CMIP6. In coastal cities, such as Istanbul, Athens, and Lisbon, these  
587 differences are likely due to the higher spatial resolution of EURO-CORDEX, which enables a better distinction of land and  
588 ocean grid cells. In other cities, like Madrid or Rome, better resolved orography might be the reason for the more frequent  
589 exceedances in EURO-CORDEX. Yet the causes for some discrepancies remain unclear, for instance for the more frequent  
590 exceedances above 30 °C projected by EURO-CORDEX for Milan, which lies in the rather flat Po Valley, or for the coastal  
591 city Barcelona, where EURO-CORDEX shows much fewer exceedances above 30 °C than CMIP5 and CMIP6.

592 In some cities, the ranking varies considerably depending on the considered heat metric (particularly in Barcelona, Oslo,  
593 Lisbon, Warsaw, and Berlin; Figure 4), indicating that the choice of metrics may strongly influence projections of ambient  
594 heat in these cities. These discrepancies in the ambient heat estimates from different heat metrics depend, for instance, on the  
595 local climate conditions, as the number of days exceeding 30 °C is strongly connected to the average summer temperatures in  
596 a city (see Figure 5a) and HWMI<sub>d</sub> values are influenced by the local temperature variability (see Eq. (1)). Additionally, in  
597 some cities the projections vary considerably within a box of 3x3 grid cells around the city centre (Supplementary Figure  
598 S4S5), especially for TX exceedances above 30 °C and HWMI<sub>d</sub>-TX. The variability is generally largest for cities located close  
599 to the sea, particularly for HWMI<sub>d</sub>-TX. This is related to the fact that HWMI<sub>d</sub>-TX values are generally much higher over the  
600 sea than on land, which is mostly due to the low climatological variability of TX<sub>x</sub> over the sea (Supplementary Figure S5S6).  
601 If cities are located close to the sea, the estimated HWMI<sub>d</sub>-TX values may thus strongly depend on how much of the grid cell  
602 located closest to the city centre is covered by land and on how much this land fraction varies across EURO-CORDEX models.  
603 In such cases, a more an accurate representation of local interactions between land and sea would be necessary (e.g., higher  
604 spatial resolution, accurate representation of advection, consideration of humidity) is necessary to generate more robust  
605 projections of ambient heat.

606 The spatial patterns of the heat metrics can largely be explained by the local temperature climatology and its projected changes  
607 (see importance of climate factors in Figure 5), with varying importance of the single explanatory factors depending on the  
608 considered metric. The explanatory factors explain most of the spatial variability in TX<sub>x</sub> change and in TX exceedances above  
609 30 °C but they only partly explain the spatial variability in HWMI<sub>d</sub>-TX. The remaining unexplained variance of the heat  
610 metrics might be connected to the amplified increase of extreme temperatures (Seneviratne et al., 2016; Vogel et al., 2017)  
611 (we use summer mean TX as explanatory factor) or asymmetric changes in the temperature distributions (we use the symmetric  
612 standard deviation of TX as explanatory factor). For HWMI<sub>d</sub>-TX, the relatively large unexplained variance might be  
613 specifically connected to the definition of HWMI<sub>d</sub>, i.e., to the usage of a cut-off temperature to define heatwaves and to the  
614 standardisation based on the climatology of TX<sub>x</sub>. The same is the case for TX exceedances above 30 °C, which are generally  
615 non-linear due to the usage of the absolute threshold of 30 °C. Among the location factors, the latitude of a city is the most  
616 important factor for explaining the spatial variance, particularly for TX exceedances above 30 °C. Generally, the explained  
617 variance is lower for location factors than for climate factors, indicating that local climate does certainly not only depend on

618 the coordinates and elevation of a location but also on other local factors, such as the predominant atmospheric circulation or  
619 local feedbacks (e.g., vegetation, soil moisture). As the contribution of the explanatory variables to the explained variance is  
620 quantified based on correlation analysis, definitive cause-effect chains cannot be deduced. Particularly for the climate factors,  
621 the results should thus rather be interpreted as an indication of the extent to which the calculated heat metrics are influenced  
622 by the underlying temperature distribution and its projected future change.

#### 623 **4.2 Limitations and potential improvements**

624 The ~12.5 km spatial resolution of the EUR-11 simulations enables a much more detailed assessment of climate variability  
625 and climate change at the city-level compared to GCMs, which have a much coarser spatial resolution (~100 km). Yet, most  
626 land surface modules of models in the 0.11° EURO-CORDEX ensemble only employ a simplified representation of urban  
627 areas (Table 1), which prevents the full exploitation of their high spatial resolution for studies focusing on urban areas. A few  
628 models represent urban areas as rock surfaces, thus neglecting the influence of urban vegetation on the surface energy balance  
629 and the influence of urban buildings on turbulence, radiation, and hydrology. Other models apply adjusted parameters (e.g.,  
630 for albedo and roughness length) and a reduced vegetation cover in urban areas, and thus consider the characteristics of cities  
631 to some extent. One of the models uses a sophisticated urban land model, which includes various aspects of urban areas, such  
632 as urban canyons, different levels of urbanisation, and radiation and hydrology schemes specifically adapted for urban areas.  
633 Despite these substantial differences in how urban areas are represented, no direct link can be found between the general  
634 behaviour of the different models in the projection of ambient heat (e.g., comparatively high levels of ambient heat in  
635 HadREM3-GA7-05 and WRF381P, and comparatively low levels in HIRHAM5, RACMO22E, and COSMO-crCLIM-v1-1,  
636 with all of these models using the adjusted-parameter approach to represent urban areas) and their representation of urban  
637 areas (Figure 8, Table 1). The CORDEX Flagship Pilot Study on URBan environments and Regional Climate Change (URB-  
638 RCC) is tackling the question of urban parameterizations and may provide important advancements for urban-resolving climate  
639 modelling in the medium term. Investing in the development of urban parameterisations might have further benefits, as their  
640 implementation in climate models may also affect regional climate outside the urban areas (Katzfey et al., 2020). -  
641 ~~YetFurthermore~~, urban temperatures usually exhibit large variability within a city, i.e., at scales that currently cannot be  
642 resolved by the 0.11° EURO-CORDEX ensemble. Urban-resolving climate modelling may provide a way forward to better  
643 quantify climate effects at scales resolving single neighbourhoods (Sharma et al., 2021; Hamdi et al., 2020), which would add  
644 valuable information for assessing the risk of heat stress due to climate change at scales relevant for local health authorities  
645 and city planners. ~~To achieve this, an adequate representation of urban land surfaces in models is essential. Yet, several land~~  
646 ~~surface modules of models in the 0.11° EURO-CORDEX ensemble do not have dedicated urban tiles or only employ a~~  
647 ~~simplified representation of urban areas. The CORDEX Flagship Pilot Study on URBan environments and Regional Climate~~  
648 ~~Change (URB-RCC) is tackling this issue and may provide important advancements for urban-resolving climate modelling in~~  
649 ~~the medium term.~~

650 ~~The reanalysis ERA5-Land does not have a dedicated urban tile either, which reduces its suitability for analysing climate at~~  
651 ~~city-level despite its high resolution of about 9 km. Investing in the development of urban parameterisations might have further~~  
652 ~~benefits, as their implementation in climate models may also affect regional climate outside the urban areas (Katzfey et al.,~~  
653 ~~2020).~~ ~~The reanalysis ERA5-Land does not have a dedicated urban tile either, which makes it less suitable for analysing climate~~  
654 ~~at city level despite its high resolution of about 9 km.~~ Moreover, the missing urban representation currently prevents the usage  
655 of ERA5-Land as a reference dataset for the application of bias adjustment to investigate urban climate. Climate data from E-  
656 OBS might reflect urban conditions to the extent weather stations are present in cities. However, weather stations are located  
657 on grassland, and E-OBS might thus underestimate ambient heat in heavily sealed parts of cities, such as city centres, inner-  
658 city residential areas, or industrial zones. In case data from paired weather stations inside a city and in its rural surroundings  
659 are available, a bias adjustment procedure for urban areas developed by Burgstall et al. (2021) can be applied to adjust climate  
660 model data to urban conditions.

661 ~~In our analysis, we do not find any pronounced UHI effects (Figure 3, Supplementary Figure S2), which is likely related to the~~  
662 ~~incomplete representation of urban areas in RCMs. As UHI is projected to only intensify gradually due to global warming~~  
663 ~~(Huang et al., 2019; Koomen and Diogo, 2017), our results for TXx change and HWMId should not be affected much by the~~  
664 ~~lack of UHI. However, the estimated exceedance rates of TX>30 °C and TN>20 °C would be impacted by UHI as they rely~~  
665 ~~on absolute temperature thresholds. As UHI might be elevated during heatwaves (Ward et al., 2016), ambient heat could be~~  
666 ~~underestimated if urban areas are not well represented in land surface modules. In addition, cities also differ in other parameters~~  
667 ~~and variables, such as roughness length and soil moisture, from the land cover that models currently use in urban areas, which~~  
668 ~~might affect our results beyond UHI.~~

669 ~~In our analysis, we do not find pronounced UHI effects (Figure 3, Supplementary Figure S3), which is likely related to the~~  
670 ~~simplified representation of urban areas in RCMs. UHI may additionally increase in the future due to global warming (Koomen~~  
671 ~~and Diogo, 2017; Tewari et al., 2019) and urban expansion (Huang et al., 2019; Koomen and Diogo, 2017), and UHI can~~  
672 ~~further be elevated during heatwaves (Ward et al., 2016). More sophisticated representations of urban areas in RCMs would~~  
673 ~~make it possible to assess how the EURO-CORDEX models project future UHI developments, and could facilitate sensitivity~~  
674 ~~studies to identify the contributions of climate change, local climate feedbacks, and urbanisation to the projected increase of~~  
675 ~~ambient heat in cities.~~

676 Differences in climate forcing or process implementation between the CMIP5, CMIP6, and EURO-CORDEX ensembles, such  
677 as differences in aerosol forcing (~~Boé et al., 2020; Gutiérrez et al., 2020; Nabat et al., 2020~~), (~~Boé et al., 2020; Gutiérrez et al.,~~  
678 ~~2020; Nabat et al., 2020~~) or diverging trends in cloudiness (Bartók et al., 2017), might further explain discrepancies in climate  
679 projections (Taranu et al., 2022). Additionally, several EURO-CORDEX models do not consider plant physiological CO<sub>2</sub>  
680 effects and thus likely underestimate extreme temperatures (Schwingshackl et al., 2019). Although the latter effect is confined  
681 to vegetated surfaces and should thus be less relevant in heavily sealed urban areas, it might still influence urban temperatures  
682 ~~if the land cover currently used by in RCMs in that consider vegetation in their representation of urban areas includes~~

683 ~~vegetation~~. This might partly explain the lower ambient heat projections of the EURO-CORDEX ensemble compared to the  
684 CMIP5 and CMIP6 ensembles, particularly in eastern and northern Europe.  
685 The usage of absolute thresholds for estimating the number of exceedance days (i.e., 30 °C for daily maximum  
686 ~~temperatures~~temperature and 20 °C for daily minimum ~~temperature~~temperature) does not reflect that temperatures vary  
687 considerably across European cities. Consequently, the number of exceedance days differs substantially across cities, showing  
688 a strong gradient from southern to northern European cities. While absolute temperature thresholds are a common metric used  
689 for projections of ambient heat (e.g., Schwingshackl et al., 2021; Zhao et al., 2015; Kjellstrom et al., 2009; Casanueva et al.,  
690 2020), epidemiological studies show continuous increases in health impacts above the locally optimal temperature (i.e., the  
691 temperature where minimal effects of health outcomes are observed, Gasparrini et al., 2015). Moreover, epidemiological  
692 studies increasingly use ~~the~~temperature ~~percentile~~percentiles as exposure metric instead of absolute temperatures ~~as exposure~~  
693 ~~metric~~ to better reflect local conditions (Masselot et al., 2023).

## 694 5 Conclusions

695 EURO-CORDEX simulations at 0.11° resolution (EUR-11, ~12.5 km) deliver climate data for Europe at a resolution that is  
696 high enough to analyse projections of ambient heat at the city-level (Figure 1). The temperature distributions of the EURO-  
697 CORDEX models generally agree with data from ERA5-Land and E-OBS in the 36 major European cities investigated, despite  
698 ~~of~~a slight TX warm bias compared to ERA5-Land, a slight TX cold bias compared to E-OBS, and a TN cold bias relative to  
699 both ERA5-Land and E-OBS (Figure 3, Supplementary Figure ~~S2~~S3).

700 Using three different metrics to quantify ambient heat at 3 °C warming in Europe relative to 1981-2010 (i.e., changes in TXx,  
701 number of days with temperatures exceeding 30 °C, and HWMI<sub>d</sub>), we find that ambient heat is projected to increase throughout  
702 the 36 major European cities investigated. Southern European cities will be particularly affected by high levels of ambient  
703 heat, but depending on the considered metric, cities in central, eastern, and northern Europe may also experience substantial  
704 increases in ambient heat (Figure 4). Nighttime HWMI<sub>d</sub> increases even more strongly than daytime HWMI<sub>d</sub> (Figure 6), with  
705 potentially severe implications for health (He et al., 2022). In several cities, the projected levels of ambient heat strongly  
706 depend on the considered metric, such as in Barcelona, Oslo, Lisbon, and Warsaw. This indicates that estimates based on a  
707 single metric might not appropriately reflect the risks of adverse health effects due to ambient heat in a warmer climate.

708 We further analyse the spatial patterns of the ambient heat projections in light of the underlying temperature climatology and  
709 its projected changes and the location of the different cities (Figure 5). Changes in TXx are mostly connected to projected  
710 changes in the mean and variability of TX, TX exceedances above 30 °C depend mostly on the average TX value in the  
711 reference period and its projected change, and the spatial patterns of HWMI<sub>d</sub> are partly explained by changes in TX and the  
712 variability in the reference period. Regarding the location of cities, latitude plays the predominant role for explaining the spatial  
713 patterns, while the other factors (longitude, elevation, location close to sea) only have limited explanatory power.



714 The EURO-CORDEX ensemble estimates lower increases in TXx and lower HWMId values than the CMIP5 and CMIP6  
715 ensembles in the majority of the analysed cities ~~at 3 °C European warming~~ (Figure 7). Yet, the EURO-CORDEX ensemble  
716 has higher TX exceedance rates of 30 °C in several cities, particularly in southern Europe. This discrepancy can be due to  
717 several factors, such as differences in forcing (Boé et al., 2020; Gutiérrez et al., 2020; Nabat et al., 2020), differences in process  
718 implementation (e.g., Bartók et al., 2017; Schwingshackl et al., 2019; Taranu et al., 2022), or the higher spatial resolution of  
719 EURO-CORDEX models being able to better represent local climate conditions. Yet, several EURO-CORDEX models ~~do not~~  
720 ~~represent~~ employ a rather simple representation of urban areas ~~(Table 1)~~, and the specific climate conditions in urban areas  
721 ~~might~~ are thus not ~~be~~ fully ~~represented~~ captured.

722 The large ensemble of 72 EURO-CORDEX simulations enables a thorough uncertainty assessment, quantified by the spread  
723 across models. The uncertainties of TXx change are generally relatively low (around 1 °C to 2 °C in all cities). For TX  
724 exceedances above 30 °C, relative uncertainties range from 20% to 60% in most southern European cities but are higher in  
725 northern European cities due to their lower TX exceedance rates of 30 °C. Applying a simple ~~bias~~ adjustment (see Section 2.3)  
726 reduces the uncertainties of the projected TX exceedances above 30 °C in all cities and yields lower exceedance rates in about  
727 40% of the cities. The estimates of ambient heat show high spatial variability around the city centre in cities located close to  
728 the shore. Particularly for HWMId, the estimates differ substantially depending on the presence of water or land in the  
729 respective grid cell (Supplementary Figure ~~S4S5~~). Accurate representations of land and sea and of their interplay are thus  
730 essential for quantifying ambient heat in coastal cities.

731 Our analysis provides an important contribution to estimate ambient heat in 36 major European cities by considering three  
732 different metrics and using data from high-resolution RCM simulations. Future studies would benefit from a more  
733 comprehensive representation of urban areas in models, which might be developed by the CORDEX Flagship Pilot Study on  
734 URbAn environments and Regional Climate Change (URB-RCC) for RCMs. ~~Systematically and completely including~~  
735 Improving the representation of urban ~~the~~ areas in the land surface modules of the EURO-CORDEX RCMs and including an  
736 urban representation in ERA5-Land would allow for an even more accurate estimation of ambient heat at the city-level. Further,  
737 the coupling of urban canopy layer models with regional climate models might pave the way for detailed analyses of heat  
738 stress in cities by combining the high spatial resolution of urban canopy layer models with the climate variability estimates  
739 from RCMs. Such ~~an analysis~~ analyses could provide an important step forward towards a comprehensive analysis of ambient  
740 heat in European cities, ~~which and worldwide, and it~~ could be combined with estimates of exposure and vulnerability to  
741 comprehensively quantify future risk of heat extremes.

742 Cities are expected to increasingly become climate hotspots due to their high population density and the local climate  
743 conditions that are partly influenced by how cities are structured. At the same time, their large innovation potential also gives  
744 cities the opportunity to lead the way in implementing climate adaptation strategies. Providing detailed and accurate data about  
745 ambient heat projections at the city-level is essential to enable cities to plan specific and effective adaptation measures against  
746 future heat extremes.

747

749 **Code availability**

750 The programming code used for the analyses and for creating the figures is available on [https://github.com/schwings-](https://github.com/schwings-clemens/ambient-heat-european-cities)  
751 [clemens/ambient-heat-european-cities](https://github.com/schwings-clemens/ambient-heat-european-cities).

752 **Data availability**

753 Data supporting this study is publicly available from <https://doi.org/10.5281/zenodo.8043755>. EURO-CORDEX, CMIP5, and  
754 CMIP6 data is available via the Earth System Grid Federation (ESGF) and can be downloaded from <https://esgf-data.dkrz.de>.  
755 ERA5-Land is available from <https://doi.org/10.24381/cds.e2161bac>. E-OBS is available from  
756 <https://doi.org/10.24381/cds.151d3ec6>. Weather station data from GSOD can be retrieved from [https://data.nodc.noaa.gov/cgi-](https://data.nodc.noaa.gov/cgi-bin/iso?id=gov.noaa.ncdc:C00516)  
757 [bin/iso?id=gov.noaa.ncdc:C00516](https://data.nodc.noaa.gov/cgi-bin/iso?id=gov.noaa.ncdc:C00516) and weather station data from ECA&D can be retrieved from <https://www.ecad.eu>.

758 **Author contributions**

759 CS and JS conceptualised the study. CI and CS curated the data. CS developed the methodology, performed the analysis, and  
760 created the visualisations. JS and KA acquired funding. CS and AD drafted the manuscript. CS, AD, CI, KA, and JS edited,  
761 ~~wrote~~, and ~~wrote~~revised the manuscript.

762 **Competing interests**

763 The authors declare that they have no conflict of interest.

764 **Acknowledgements**

765 We thank Nina Schuhen for her support with the statistical analysis, particularly regarding the quantification of how much the  
766 different explanatory factors can explain the observed spatial patterns of ambient heat. We further thank Marit Sandstad for  
767 processing the ERA5-Land data. We acknowledge the E-OBS dataset and the data providers in the ECA&D project  
768 (<https://www.ecad.eu>). This study contains modified Copernicus Climate Change Service information [2022]. We  
769 acknowledge the World Climate Research Programme's Working Group on Coupled Modelling, which is responsible for  
770 CMIP, the World Climate Research Programme's Working Group on Regional Climate, and the Working Group on Coupled  
771 Modelling, former coordinating body of CORDEX and responsible panel for CMIP5. We thank the climate modelling groups  
772 for producing and making available their model output, the Earth System Grid Federation (ESGF) for archiving the data and

773 providing access, and the multiple funding agencies who support CMIP5, CMIP6 and ESGF. We also acknowledge the Earth  
774 System Grid Federation infrastructure, an international effort led by the US Department of Energy's Program for Climate  
775 Model Diagnosis and Intercomparison, the European Network for Earth System Modelling and other partners in the Global  
776 Organisation for Earth System Science Portals (GO-ESSP). For CMIP the US Department of Energy's Program for Climate  
777 Model Diagnosis and Intercomparison provides coordinating support and led development of software infrastructure in  
778 partnership with the Global Organization for Earth System Science Portals.

779 This work has received funding from the European Union's Horizon 2020 research and innovation program under grant  
780 agreement No 820655 (EXHAUSTION) and from the Belmont Forum Collaborative Research Action on Climate,  
781 Environment, and Health, supported by the Research Council of Norway (contract No 310672, HEATCOST). Jana Sillmann  
782 and Anne Sophie Daloz were supported through the CICERO Strategic Project on Climate Change Risk (no. 160015/F40),  
783 funded by the Research Council of Norway.

784

785 **References**

- 786 Alizadeh, M. R., Abatzoglou, J. T., Adamowski, J. F., Prestemon, J. P., Chittoori, B., Akbari Asanjan, A., and Sadegh, M.:  
787 Increasing Heat-Stress Inequality in a Warming Climate, *Earths Future*, 10, <https://doi.org/10.1029/2021EF002488>, 2022.
- 788 Argueso, D., Evans, J. P., Pitman, A. J., and Di Luca, A.: Effects of city expansion on heat stress under climate change  
789 conditions, *PLOS ONE*, 10, e0117066, <https://doi.org/10.1371/journal.pone.0117066>, 2015.
- 790 [Armstrong, B., Sera, F., Vicedo-Cabrera, A. M., Abrutzky, R., Åström, D. O., Bell, M. L., Chen, B.-Y., de Sousa Zanotti](#)  
791 [Stagliorio Coelho, M., Correa, P. M., Dang, T. N., Diaz, M. H., Dung, D. V., Forsberg, B., Goodman, P., Guo, Y.-L. L., Guo,](#)  
792 [Y., Hashizume, M., Honda, Y., Indermitte, E., Íñiguez, C., Kan, H., Kim, H., Kyselý, J., Lavigne, E., Michelozzi, P., Orru, H.,](#)  
793 [Ortega, N. V., Pascal, M., Ragetli, M. S., Saldiva, P. H. N., Schwartz, J., Scortichini, M., Seposo, X., Tobias, A., Tong, S.,](#)  
794 [Urban, A., la Cruz Valencia, C. D., Zanobetti, A., Zeka, A., and Gasparrini, A.: The Role of Humidity in Associations of High](#)  
795 [Temperature with Mortality: A Multicountry, Multicity Study, \*Environ. Health Perspect.\*, 127, 097007–097007,](#)  
796 [<https://doi.org/10.1289/EHP5430>, 2019.](#)
- 797 Åström, D. O., Forsberg, B., Edvinsson, S., and Rocklöv, J.: Acute Fatal Effects of Short-Lasting Extreme Temperatures in  
798 Stockholm, Sweden: Evidence Across a Century of Change, *Epidemiology*, 24, 820–829,  
799 <https://doi.org/10.1097/01.ede.0000434530.62353.0b>, 2013.
- 800 Azen, R. and Budescu, D. V.: The dominance analysis approach for comparing predictors in multiple regression., *Psychol.*  
801 *Methods*, 8, 129–129, <https://doi.org/10.1037/1082-989X.8.2.129>, 2003.
- 802 Bartók, B., Wild, M., Folini, D., Lüthi, D., Kotlarski, S., Schär, C., Vautard, R., Jerez, S., and Imecs, Z.: Projected changes in  
803 surface solar radiation in CMIP5 global climate models and in EURO-CORDEX regional climate models for Europe, *Clim.*  
804 *Dyn.*, 49, 2665–2683–2665–2683, <https://doi.org/10.1007/s00382-016-3471-2>, 2017.
- 805 [Best, M. J., Pryor, M., Clark, D. B., Rooney, G. G., Essery, R. . L. H., Ménard, C. B., Edwards, J. M., Hendry, M. A., Porson,](#)  
806 [A., Gedney, N., Mercado, L. M., Sitch, S., Blyth, E., Boucher, O., Cox, P. M., Grimmond, C. S. B., and Harding, R. J.: The](#)  
807 [Joint UK Land Environment Simulator \(JULES\), model description – Part 1: Energy and water fluxes, \*Geosci. Model Dev.\*,](#)  
808 [4, 677–699, <https://doi.org/10.5194/gmd-4-677-2011>, 2011.](#)
- 809 Boé, J., Somot, S., Corre, L., and Nabat, P.: Large discrepancies in summer climate change over Europe as projected by global  
810 and regional climate models: causes and consequences, *Clim. Dyn.*, 54, 2981–3002, <https://doi.org/10.1007/s00382-020->  
811 [05153-1](#), 2020.
- 812 Burgstall, A., Kotlarski, S., Casanueva, A., Hertig, E., Fischer, E., and Knutti, R.: Urban multi-model climate projections of  
813 intense heat in Switzerland, *Clim. Serv.*, 22, 100228, <https://doi.org/10.1016/j.cliser.2021.100228>, 2021.
- 814 Casanueva, A., Kotlarski, S., Fischer, A. M., Flouris, A. D., Kjellstrom, T., Lemke, B., Nybo, L., Schwierz, C., and Liniger,  
815 M. A.: Escalating environmental summer heat exposure—a future threat for the European workforce, *Reg. Environ. Change*,  
816 20, <https://doi.org/10.1007/s10113-020-01625-6>, 2020.
- 817 Chapman, S., Thatcher, M., Salazar, A., Watson, J. E. M., and McAlpine, C. A.: The impact of climate change and urban  
818 growth on urban climate and heat stress in a subtropical city, *Int. J. Climatol.*, 39, 3013–3030, <https://doi.org/10.1002/joc.5998>,  
819 2019.
- 820 [Chen, F., Kusaka, H., Bornstein, R., Ching, J., Grimmond, C. S. B., Grossman-Clarke, S., Loridan, T., Manning, K. W.,](#)  
821 [Martilli, A., Miao, S., Sailor, D., Salamanca, F. P., Taha, H., Tewari, M., Wang, X., Wyszogrodzki, A. A., and Zhang, C.: The](#)

- 822 [integrated WRF/urban modelling system: development, evaluation, and applications to urban environmental problems, \*Int. J.\*](#)  
823 [Climatol., 31, 273–288, <https://doi.org/10.1002/joc.2158>, 2011.](#)
- 824 Coppola, E., Nogherotto, R., Ciarlo, J. M., Giorgi, F., Meijgaard, E., Kadygrov, N., Iles, C., Corre, L., Sandstad, M., Somot,  
825 S., Nabat, P., Vautard, R., Levavasseur, G., Schwingshackl, C., Sillmann, J., Kjellström, E., Nikulin, G., Aalbers, E.,  
826 Lenderink, G., Christensen, O. B., Boberg, F., Sørland, S. L., Demory, M.-E., Bülow, K., Teichmann, C., Warrach-Sagi, K.,  
827 and Wulfmeyer, V.: Assessment of the European Climate Projections as Simulated by the Large EURO-CORDEX Regional  
828 and Global Climate Model Ensemble, *J. Geophys. Res. Atmospheres*, 126, <https://doi.org/10.1029/2019jd032356>, 2021.
- 829 Cornes, R. C., van der Schrier, G., van den Besselaar, E. J. M., and Jones, P. D.: An Ensemble Version of the E-OBS  
830 Temperature and Precipitation Data Sets, *J. Geophys. Res. Atmospheres*, 123, 9391–9409,  
831 <https://doi.org/10.1029/2017jd028200>, 2018.
- 832 [Daniel, M., Lemonsu, A., Déqué, M., Somot, S., Alias, A., and Masson, V.: Benefits of explicit urban parameterization in](#)  
833 [regional climate modeling to study climate and city interactions, \*Clim. Dyn.\*, 52, 2745–2764, \[https://doi.org/10.1007/s00382-\]\(https://doi.org/10.1007/s00382-018-4289-x\)](#)  
834 [018-4289-x](#), 2018.
- 835 [Decharme, B., Delire, C., Minvielle, M., Colin, J., Vergnes, J., Alias, A., Saint-Martin, D., Séférian, R., Sénési, S., and](#)  
836 [Voldoire, A.: Recent Changes in the ISBA-CTRIP Land Surface System for Use in the CNRM-CM6 Climate Model and in](#)  
837 [Global Off-Line Hydrological Applications, \*J. Adv. Model. Earth Syst.\*, 11, 1207–1252,](#)  
838 <https://doi.org/10.1029/2018MS001545>, 2019.
- 839 [Doms, G., Förstner, J., Heise, E., Herzog, H. J., Mironov, D., Raschendorfer, M., Reinhardt, T., Ritter, B., Schrodin, R., Schulz,](#)  
840 [J.-P., and others: A description of the nonhydrostatic regional COSMO model. Part II: physical parameterization, \*Dtsch.\*](#)  
841 [Wetterd. Offenb. Ger., 2011.](#)
- 842 Dosio, A., Mentaschi, L., Fischer, E. M., and Wyser, K.: Extreme heat waves under 1.5 °C and 2 °C global warming, *Environ.*  
843 *Res. Lett.*, 13, 054006, <https://doi.org/10.1088/1748-9326/aab827>, 2018.
- 844 [ECMWF: IFS Documentation CY45R1 - Part IV : Physical processes, <https://doi.org/10.21957/4WHWO8JW0>, 2018.](#)
- 845 Fischer, E. M. and Schär, C.: Consistent geographical patterns of changes in high-impact European heatwaves, *Nat. Geosci.*,  
846 3, 398–398, <https://doi.org/10.1038/ngeo866>, 2010.
- 847 Forzieri, G., Feyen, L., Russo, S., Vousdoukas, M., Alfieri, L., Outten, S., Migliavacca, M., Bianchi, A., Rojas, R., and Cid,  
848 A.: Multi-hazard assessment in Europe under climate change, *Clim. Change*, 137, 105–119, [https://doi.org/10.1007/s10584-](https://doi.org/10.1007/s10584-016-1661-x)  
849 [016-1661-x](#), 2016.
- 850 [de Freitas, C. R. and Grigorieva, E. A.: A comparison and appraisal of a comprehensive range of human thermal climate](#)  
851 [indices, \*Int. J. Biometeorol.\*, 61, 487-512-487–512, <https://doi.org/10.1007/s00484-016-1228-6>, 2017.](#)
- 852 Freychet, N., Hegerl, G. C., Lord, N. S., Lo, Y. T. E., Mitchell, D., and Collins, M.: Robust increase in population exposure to  
853 heat stress with increasing global warming, *Environ. Res. Lett.*, 17, 064049, <https://doi.org/10.1088/1748-9326/ac71b9>, 2022.
- 854 [Garbero, V., Milelli, M., Bucchignani, E., Mercogliano, P., Varentsov, M., Rozinkina, I., Rivin, G., Blinov, D., Wouters, H.,](#)  
855 [Schulz, J.-P., Schättler, U., Bassani, F., Demuzere, M., and Repola, F.: Evaluating the Urban Canopy Scheme TERRA\\_URB](#)  
856 [in the COSMO Model for Selected European Cities, \*Atmosphere\*, 12, 237, <https://doi.org/10.3390/atmos12020237>, 2021.](#)
- 857 García-León, D., Casanueva, A., Standardi, G., Burgstall, A., Flouris, A. D., and Nybo, L.: Current and projected regional  
858 economic impacts of heatwaves in Europe, *Nat. Commun.*, 12, 5807, <https://doi.org/10.1038/s41467-021-26050-z>, 2021.

- 859 Gasparrini, A., Guo, Y., Hashizume, M., Lavigne, E., Zanobetti, A., Schwartz, J., Tobias, A., Tong, S., Rocklöv, J., Forsberg,  
860 B., Leone, M., De Sario, M., Bell, M. L., Guo, Y.-L. L., Wu, C., Kan, H., Yi, S.-M., de Sousa Zanotti Stagliorio Coelho, M.,  
861 Saldiva, P. H. N., Honda, Y., Kim, H., and Armstrong, B.: Mortality risk attributable to high and low ambient temperature: a  
862 multicountry observational study, *The Lancet*, 386, 369–375, [https://doi.org/10.1016/S0140-6736\(14\)62114-0](https://doi.org/10.1016/S0140-6736(14)62114-0), 2015.
- 863 Gasparrini, A., Guo, Y., Sera, F., Vicedo-Cabrera, A. M., Huber, V., Tong, S., de Sousa Zanotti Stagliorio Coelho, M., Saldiva,  
864 P. H. N., Lavigne, E., Correa, P. M., Ortega, N. V., Kan, H., Osorio, S., Kysely, J., Urban, A., Jaakkola, J. J. K., Rytö, N. R. I.,  
865 Pascal, M., Goodman, P. G., Zeka, A., Michelozzi, P., Scortichini, M., Hashizume, M., Honda, Y., Hurtado-Díaz, M., Cruz, J.  
866 C., Seposo, X., Kim, H., Tobias, A., Iñiguez, C., Forsberg, B., Åström, D. O., Ragettli, M. S., Guo, Y. L., Wu, C., Zanobetti,  
867 A., Schwartz, J., Bell, M. L., Dang, T. N., Van, D. D., Heaviside, C., Vardoulakis, S., Hajat, S., Haines, A., and Armstrong,  
868 B.: Projections of temperature-related excess mortality under climate change scenarios, *Lancet Planet. Health*, 1, e360-e367-  
869 e360–e367, [https://doi.org/10.1016/S2542-5196\(17\)30156-0](https://doi.org/10.1016/S2542-5196(17)30156-0), 2017.
- 870 Goret, M., Masson, V., Schoetter, R., and Moine, M.-P.: Inclusion of CO<sub>2</sub> flux modelling in an urban canopy layer model and  
871 an evaluation over an old European city centre, *Atmospheric Environ.* X, 3, 100042,  
872 <https://doi.org/10.1016/j.aeaoa.2019.100042>, 2019.
- 873 Guerreiro, S. B., Dawson, R. J., Kilsby, C., Lewis, E., and Ford, A.: Future heat-waves, droughts and floods in 571 European  
874 cities, *Environ. Res. Lett.*, 13, <https://doi.org/10.1088/1748-9326/aaaad3>, 2018.
- 875 Gutiérrez, C., Somot, S., Nabat, P., Mallet, M., Corre, L., Meijgaard, E. van, Perpiñán, O., and Gaertner, M. Á.: Future  
876 evolution of surface solar radiation and photovoltaic potential in Europe: investigating the role of aerosols, *Environ. Res. Lett.*,  
877 15, 034035, <https://doi.org/10.1088/1748-9326/ab6666>, 2020.
- 878 [Hagemann, S.: An improved land surface parameter dataset for global and regional climate models, 2002.](#)
- 879 Hamdi, R., Kusaka, H., Doan, Q.-V., Cai, P., He, H., Luo, G., Kuang, W., Caluwaerts, S., Duchêne, F., Van Schaeybroek, B.,  
880 and Termonia, P.: The State-of-the-Art of Urban Climate Change Modeling and Observations, *Earth Syst. Environ.*, 4, 631–  
881 646, <https://doi.org/10.1007/s41748-020-00193-3>, 2020.
- 882 He, C., Kim, H., Hashizume, M., Lee, W., Honda, Y., Kim, S. E., Kinney, P. L., Schneider, A., Zhang, Y., Zhu, Y., Zhou, L.,  
883 Chen, R., and Kan, H.: The effects of night-time warming on mortality burden under future climate change scenarios: a  
884 modelling study, *Lancet Planet. Health*, 6, e648–e657, [https://doi.org/10.1016/S2542-5196\(22\)00139-5](https://doi.org/10.1016/S2542-5196(22)00139-5), 2022.
- 885 Heaviside, C., Macintyre, H., and Vardoulakis, S.: The Urban Heat Island: Implications for Health in a Changing Environment,  
886 *Curr Env. Health Rep*, 4, 296–305, <https://doi.org/10.1007/s40572-017-0150-3>, 2017.
- 887 Huang, K., Li, X., Liu, X., and Seto, K. C.: Projecting global urban land expansion and heat island intensification through  
888 2050, *Environ. Res. Lett.*, 14, 114037, <https://doi.org/10.1088/1748-9326/ab4b71>, 2019.
- 889 Iles, C. E., Vautard, R., Strachan, J., Joussaume, S., Eggen, B. R., and Hewitt, C. D.: The benefits of increasing resolution in  
890 global and regional climate simulations for European climate extremes, *Geosci. Model Dev.*, 13, 5583–5607,  
891 <https://doi.org/10.5194/gmd-13-5583-2020>, 2020.
- 892 IPCC: Climate Change 2021: The Physical Science Basis. Contribution of Working Group I to the Sixth Assessment Report  
893 of the Intergovernmental Panel on Climate Change, Cambridge University Press, Cambridge, United Kingdom and New York,  
894 NY, USA, 2021.
- 895 IPCC: Climate Change 2022: Impacts, Adaptation and Vulnerability. Contribution of Working Group II to the Sixth  
896 Assessment Report of the Intergovernmental Panel on Climate Change, edited by: H.-O. Pörtner, B. R., D. C. Roberts, M.

- 897 Tignor, E. S. Poloczanska, K. Mintenbeck, A. Alegría, M. Craig, S. Langsdorf, S. Löschke, V. Möller, A. Okem, Cambridge  
898 University Press, Cambridge, UK and New York, NY, USA, <https://doi.org/10.1017/9781009325844.001>, 2022.
- 899 [Jacob, D., Elizalde, A., Haensler, A., Hagemann, S., Kumar, P., Podzun, R., Rechid, D., Remedio, A. R., Saeed, F., Sieck, K.,  
900 Teichmann, C., and Wilhelm, C.: Assessing the Transferability of the Regional Climate Model REMO to Different  
901 COordinated Regional Climate Downscaling EXperiment \(CORDEX\) Regions, \*Atmosphere\*, 3, 181–199,  
902 <https://doi.org/10.3390/atmos3010181>, 2012.](https://doi.org/10.3390/atmos3010181)
- 903 [Jacob, D., Petersen, J., Eggert, B., Alias, A., Christensen, O. B., Bouwer, L. M., Braun, A., Colette, A., Déqué, M., Georgievski,  
904 G., Georgopoulou, E., Gobiet, A., Menut, L., Nikulin, G., Haensler, A., Hempelmann, N., Jones, C., Keuler, K., Kovats, S.,  
905 Kröner, N., Kotlarski, S., Kriegsman, A., Martin, E., van Meijgaard, E., Moseley, C., Pfeifer, S., Preuschmann, S.,  
906 Radermacher, C., Radtke, K., Rechid, D., Rounsevell, M., Samuelsson, P., Somot, S., Soussana, J.-F., Teichmann, C.,  
907 Valentini, R., Vautard, R., Weber, B., and Yiou, P.: EURO-CORDEX: new high-resolution climate change projections for  
908 European impact research, \*Reg. Environ. Change\*, 14, 563–578, <https://doi.org/10.1007/s10113-013-0499-2>, 2013.](https://doi.org/10.1007/s10113-013-0499-2)
- 909 Junk, J., Goergen, K., and Krein, A.: Future Heat Waves in Different European Capitals Based on Climate Change Indicators,  
910 *Int J Env. Res Public Health*, 16, <https://doi.org/10.3390/ijerph16203959>, 2019.
- 911 Karwat, A. and Franzke, C. L. E.: Future Projections of Heat Mortality Risk for Major European Cities, *Weather Clim. Soc.*,  
912 <https://doi.org/10.1175/WCAS-D-20-0142.1>, 2021.
- 913 Katzfey, J., Schlünzen, H., Hoffmann, P., and Thatcher, M.: How an urban parameterization affects a high-resolution global  
914 climate simulation, *Q. J. R. Meteorol. Soc.*, 146, 3808–3829, <https://doi.org/10.1002/qj.3874>, 2020.
- 915 Keat, W. J., Kendon, E. J., and Bohnenstengel, S. I.: Climate change over UK cities: the urban influence on extreme  
916 temperatures in the UK climate projections, *Clim. Dyn.*, 57, 3583–3597, <https://doi.org/10.1007/s00382-021-05883-w>, 2021.
- 917 [Kent, S. T., McClure, L. A., Zaitchik, B. F., Smith, T. T., and Gohlke, J. M.: Heat Waves and Health Outcomes in Alabama  
918 \(USA\): The Importance of Heat Wave Definition, \*Environ. Health Perspect.\*, 122, 151-158-151–158,  
919 <https://doi.org/10.1289/ehp.1307262>, 2014.](https://doi.org/10.1289/ehp.1307262)
- 920 Kjellstrom, T., Kovats, R. S., Lloyd, S. J., Holt, T., and Tol, R. S. J.: The Direct Impact of Climate Change on Regional Labor  
921 Productivity, *Arch. Environ. Occup. Health*, 64, 217-227-217–227, <https://doi.org/10.1080/19338240903352776>, 2009.
- 922 Klein Tank, A. M. G., Wijngaard, J. B., Können, G. P., Böhm, R., Demarée, G., Gocheva, A., Miletta, M., Pashiardis, S.,  
923 Hejkrlik, L., Kern-Hansen, C., Heino, R., Bessemoulin, P., Müller-Westermeier, G., Tzanakou, M., Szalai, S., Pálsdóttir, T.,  
924 Fitzgerald, D., Rubin, S., Capaldo, M., Maugeri, M., Leitass, A., Bukantis, A., Aberfeld, R., van Engelen, A. F. V., Forland,  
925 E., Miletus, M., Coelho, F., Mares, C., Razuvaev, V., Nieplova, E., Cegnar, T., Antonio López, J., Dahlström, B., Moberg, A.,  
926 Kirchofer, W., Ceylan, A., Pachaliuk, O., Alexander, L. V., and Petrovic, P.: Daily dataset of 20th-century surface air  
927 temperature and precipitation series for the European Climate Assessment, *Int. J. Climatol.*, 22, 1441–1453,  
928 <https://doi.org/10.1002/joc.773>, 2002.
- 929 Klok, E. J. and Klein Tank, A. M. G.: Updated and extended European dataset of daily climate observations, *Int. J. Climatol.*,  
930 29, 1182–1191, <https://doi.org/10.1002/joc.1779>, 2009.
- 931 Koomen, E. and Diogo, V.: Assessing potential future urban heat island patterns following climate scenarios, socio-economic  
932 developments and spatial planning strategies, *Mitig. Adapt. Strateg. Glob. Change*, 22, 287–306,  
933 <https://doi.org/10.1007/s11027-015-9646-z>, 2017.

- 934 Krayenhoff, E. S., Jiang, T., Christen, A., Martilli, A., Oke, T. R., Bailey, B. N., Nazarian, N., Voogt, J. A., Giometto, M. G.,  
935 Stastny, A., and Crawford, B. R.: A multi-layer urban canopy meteorological model with trees (BEP-Tree): Street tree impacts  
936 on pedestrian-level climate, *Urban Clim.*, 32, 100590, <https://doi.org/10.1016/j.uclim.2020.100590>, 2020.
- 937 Kusaka, H., Hara, M., and Takane, Y.: Urban Climate Projection by the WRF Model at 3-km Horizontal Grid Increment:  
938 Dynamical Downscaling and Predicting Heat Stress in the 2070's August for Tokyo, Osaka, and Nagoya Metropolises, *J.*  
939 *Meteorol. Soc. Jpn. Ser II*, 90B, 47–63, <https://doi.org/10.2151/jmsj.2012-B04>, 2012.
- 940 Langendijk, G. S., Rechid, D., and Jacob, D.: Urban Areas and Urban–Rural Contrasts under Climate Change: What Does the  
941 EURO-CORDEX Ensemble Tell Us?—Investigating near Surface Humidity in Berlin and Its Surroundings, *Atmosphere*, 10,  
942 <https://doi.org/10.3390/atmos10120730>, 2019.
- 943 Li, C., Zwiers, F., Zhang, X., Li, G., Sun, Y., and Wehner, M.: Changes in Annual Extremes of Daily Temperature and  
944 Precipitation in CMIP6 Models, *J. Clim.*, 34, 3441–3460, <https://doi.org/10.1175/JCLI-D-19-1013.1>, 2021.
- 945 Li, D. and Bou-Zeid, E.: Synergistic Interactions between Urban Heat Islands and Heat Waves: The Impact in Cities Is Larger  
946 than the Sum of Its Parts, *J. Appl. Meteorol. Climatol.*, 52, 2051–2064, <https://doi.org/10.1175/jamc-d-13-02.1>, 2013.
- 947 Lin, C., Kjellström, E., Wilcke, R. A. I., and Chen, D.: Present and future European heat wave magnitudes: climatologies,  
948 trends, and their associated uncertainties in GCM-RCM model chains, *Earth Syst. Dyn.*, 13, 1197–1214,  
949 <https://doi.org/10.5194/esd-13-1197-2022>, 2022.
- 950 Lundgren, K., Kuklane, K., Gao, C., and HOLM<sup>^</sup>^Eacute;R, I.: Effects of Heat Stress on Working Populations when Facing  
951 Climate Change, *Ind. Health*, 51, 3–15, <https://doi.org/10.2486/indhealth.2012-0089>, 2013.
- 952 Maraun, D.: Bias Correcting Climate Change Simulations - a Critical Review, *Curr. Clim. Change Rep.*, 2, 211-220-211–220,  
953 <https://doi.org/10.1007/s40641-016-0050-x>, 2016.
- 954 Masselot, P., Mistry, M., Vanoli, J., Schneider, R., Jungman, T., Garcia-Leon, D., Ciscar, J.-C., Feyen, L., Orru, H., Urban,  
955 A., Breitner, S., Huber, V., Schneider, A., Samoli, E., Stafoggia, M., de' Donato, F., Rao, S., Armstrong, B., Nieuwenhuijsen,  
956 M., Vicedo-Cabrera, A. M., Gasparrini, A., Achilleos, S., Kyselý, J., Indermitte, E., Jaakkola, J. J. K., Rytí, N., Pascal, M.,  
957 Katsouyanni, K., Analitis, A., Goodman, P., Zeka, A., Michelozzi, P., Houthuijs, D., Ameling, C., Rao, S., das Neves Pereira  
958 da Silva, S., Madureira, J., Holobaca, I.-H., Tobias, A., Íñiguez, C., Forsberg, B., Åström, C., Ragetti, M. S., Analitis, A.,  
959 Katsouyanni, K., Surname, F. name, Zafeiratou, S., Vazquez Fernandez, L., Monteiro, A., Rai, M., Zhang, S., and Anan, K.:  
960 Excess mortality attributed to heat and cold: a health impact assessment study in 854 cities in Europe, *Lancet Planet. Health*,  
961 7, e271–e281, [https://doi.org/10.1016/S2542-5196\(23\)00023-2](https://doi.org/10.1016/S2542-5196(23)00023-2), 2023.
- 962 Masson, V., Lemonsu, A., Hidalgo, J., and Voogt, J.: Urban Climates and Climate Change, *Annu. Rev. Environ. Resour.*, 45,  
963 411–444, <https://doi.org/10.1146/annurev-environ-012320-083623>, 2020.
- 964 McMichael, A. J., Woodruff, R. E., and Hales, S.: Climate change and human health: present and future risks, *The Lancet*,  
965 367, 859-869-859–869, [https://doi.org/10.1016/S0140-6736\(06\)68079-3](https://doi.org/10.1016/S0140-6736(06)68079-3), 2006.
- 966 [van Meijgaard, E., Van Ulft, L., Van de Berg, W., Bosveld, F., Van den Hurk, B., Lenderink, G., and Siebesma, A.: The KNMI](#)  
967 [regional atmospheric climate model RACMO, version 2.1, KNMI De Bilt, The Netherlands, 2008.](#)
- 968 Molina, M. O., Sanchez, E., and Gutierrez, C.: Future heat waves over the Mediterranean from an Euro-CORDEX regional  
969 climate model ensemble, *Sci Rep*, 10, 8801, <https://doi.org/10.1038/s41598-020-65663-0>, 2020.



- 970 Muñoz-Sabater, J., Dutra, E., Agustí-Panareda, A., Albergel, C., Arduini, G., Balsamo, G., Boussetta, S., Choulga, M.,  
971 Harrigan, S., Hersbach, H., Martens, B., Miralles, D. G., Piles, M., Rodríguez-Fernández, N. J., Zsoter, E., Buontempo, C.,  
972 and Thépaut, J.-N.: ERA5-Land: a state-of-the-art global reanalysis dataset for land applications, *Earth Syst. Sci. Data*, 13,  
973 4349–4383, <https://doi.org/10.5194/essd-13-4349-2021>, 2021.
- 974 Nabat, P., Somot, S., Cassou, C., Mallet, M., Michou, M., Bouniol, D., Decharme, B., Drugé, T., Roehrig, R., and Saint-  
975 Martin, D.: Modulation of radiative aerosols effects by atmospheric circulation over the Euro-Mediterranean region,  
976 *Atmospheric Chem. Phys.*, 20, 8315–8349, <https://doi.org/10.5194/acp-20-8315-2020>, 2020.
- 977 [Niu, G.-Y., Yang, Z.-L., Mitchell, K. E., Chen, F., Ek, M. B., Barlage, M., Kumar, A., Manning, K., Niyogi, D., Rosero, E.,  
978 Tewari, M., and Xia, Y.: The community Noah land surface model with multiparameterization options \(Noah-MP\): 1. Model  
979 description and evaluation with local-scale measurements, \*J. Geophys. Res.\*, 116, D12109,  
980 <https://doi.org/10.1029/2010JD015139>, 2011.](https://doi.org/10.1029/2010JD015139)
- 981 [Oleson, K., Bonan, G., Feddema, J., Vertenstein, M., and Kluzek, E.: Technical Description of an Urban Parameterization for  
982 the Community Land Model \(CLMU\), UCAR/NCAR, <https://doi.org/10.5065/D6K35RM9>, 2010.](https://doi.org/10.5065/D6K35RM9)
- 983 [Oleson, K., Lawrence, D., Bonan, G., Drewniak, B., Huang, M., Koven, C., Levis, S., Li, F., Riley, W., Subin, Z., Swenson,  
984 S., Thornton, P., Bozbiyik, A., Fisher, R., Heald, C., Kluzek, E., Lamarque, J.-F., Lawrence, P., Leung, L., Lipscomb, W.,  
985 Muszala, S., Ricciuto, D., Sacks, W., Sun, Y., Tang, J., and Yang, Z.-L.: Technical description of version 4.5 of the Community  
986 Land Model \(CLM\), UCAR/NCAR, <https://doi.org/10.5065/D6RR1W7M>, 2013.](https://doi.org/10.5065/D6RR1W7M)
- 987 [Oleson, K. W. and Feddema, J.: Parameterization and Surface Data Improvements and New Capabilities for the Community  
988 Land Model Urban \(CLMU\), \*J. Adv. Model. Earth Syst.\*, 12, e2018MS001586, <https://doi.org/10.1029/2018MS001586>, 2020.](https://doi.org/10.1029/2018MS001586)
- 989 Orlov, A., Daloz, A. S., Sillmann, J., Thiery, W., Douzal, C., Lejeune, Q., and Schleussner, C.: Global Economic Responses  
990 to Heat Stress Impacts on Worker Productivity in Crop Production, *Econ. Disasters Clim. Change*, 5, 367–390,  
991 <https://doi.org/10.1007/s41885-021-00091-6>, 2021.
- 992 Perkins, S. E.: A review on the scientific understanding of heatwaves—Their measurement, driving mechanisms, and changes  
993 at the global scale, *Atmospheric Res.*, 164–165, 242–267–242–267, <https://doi.org/10.1016/j.atmosres.2015.05.014>, 2015.
- 994 Perkins, S. E. and Alexander, L. V.: On the Measurement of Heat Waves, *J. Clim.*, 26, 4500–4517,  
995 <https://doi.org/10.1175/JCLI-D-12-00383.1>, 2013.
- 996 Perkins-Kirkpatrick, S. E. and Lewis, S. C.: Increasing trends in regional heatwaves, *Nat. Commun.*, 11, 3357,  
997 <https://doi.org/10.1038/s41467-020-16970-7>, 2020.
- 998 Petkova, E. P., Gasparrini, A., and Kinney, P. L.: Heat and Mortality in New York City Since the Beginning of the 20th  
999 Century., *Epidemiology*, 25, 554–560, <https://doi.org/10.1097/EDE.000000000000123>, 2014.
- 1000 Ramamurthy, P. and Bou-Zeid, E.: Heatwaves and urban heat islands: A comparative analysis of multiple cities, *J. Geophys.*  
1001 *Res. Atmospheres*, 122, 168–178, <https://doi.org/10.1002/2016jd025357>, 2017.
- 1002 [Remedio, A. R., Teichmann, C., Buntmeyer, L., Sieck, K., Weber, T., Rechid, D., Hoffmann, P., Nam, C., Kotova, L., and  
1003 Jacob, D.: Evaluation of New CORDEX Simulations Using an Updated Köppen–Trewartha Climate Classification,  
1004 \*Atmosphere\*, 10, 726, <https://doi.org/10.3390/atmos10110726>, 2019.](https://doi.org/10.3390/atmos10110726)

- 1005 [Roeckner, E., Arpe, K., Bengtsson, L., Christoph, M., Claussen, M., Dümenil, L., Esch, M., Giorgetta, M., Schlese, U., and](#)  
1006 [Schulzweida, U.: The atmospheric general circulation model ECHAM4: Model description and simulation of present day](#)  
1007 [climate, 1996.](#)
- 1008 [Roeckner, E., Bäuml, G., Bonaventura, L., Brokopf, R., Esch, M., Giorgetta, M., Hagemann, S., Kirchner, I., Kornbluh, L.,](#)  
1009 [Manzini, E., and others: The atmospheric general circulation model ECHAM5. PART I: Model description, 2003.](#)
- 1010 Royé, D., Sera, F., Tobias, A., Lowe, R., Gasparrini, A., Pascal, M., de' Donato, F., Nunes, B., and Teixeira, J. P.: Effects of  
1011 Hot Nights on Mortality in Southern Europe, *Epidemiology*, 32, 487–498, <https://doi.org/10.1097/EDE.0000000000001359>,  
1012 2021.
- 1013 Russo, S., Sillmann, J., and Fischer, E. M.: Top ten European heatwaves since 1950 and their occurrence in the coming decades,  
1014 *Environ. Res. Lett.*, 10, <https://doi.org/10.1088/1748-9326/10/12/124003>, 2015.
- 1015 Russo, S., Sillmann, J., and Sterl, A.: Humid heat waves at different warming levels, *Sci. Rep.*, 7, 7477–7477,  
1016 <https://doi.org/10.1038/s41598-017-07536-7>, 2017.
- 1017 [Samuelsson, P., Gollvik, S., Kupiainen, M., Kourzeneva, E., and van de Berg, W. J.: The surface processes of the Rossby](#)  
1018 [Centre regional atmospheric climate model \(RCA4\), SMHI, 2015.](#)
- 1019 Schwingshackl, C., Hirschi, M., and Seneviratne, S. I.: Global Contributions of Incoming Radiation and Land Surface  
1020 Conditions to Maximum Near-Surface Air Temperature Variability and Trend, *Geophys Res Lett*, 45, 5034–5044,  
1021 <https://doi.org/10.1029/2018GL077794>, 2018.
- 1022 Schwingshackl, C., Davin, E. L., Hirschi, M., Sørland, S. L., Wartenburger, R., and Seneviratne, S. I.: Regional climate model  
1023 projections underestimate future warming due to missing plant physiological CO<sub>2</sub> response, *Environ. Res. Lett.*, 14,  
1024 <https://doi.org/10.1088/1748-9326/ab4949>, 2019.
- 1025 Schwingshackl, C., Sillmann, J., Vicedo-Cabrera, A. M., Sandstad, M., and Aunan, K.: Heat Stress Indicators in CMIP6:  
1026 Estimating Future Trends and Exceedances of Impact-Relevant Thresholds, *Earths Future*, 9,  
1027 <https://doi.org/10.1029/2020ef001885>, 2021.
- 1028 Seneviratne, S. I. and Hauser, M.: Regional Climate Sensitivity of Climate Extremes in CMIP6 Versus CMIP5 Multimodel  
1029 Ensembles, *Earths Future*, 8, <https://doi.org/10.1029/2019EF001474>, 2020.
- 1030 Seneviratne, S. I., Donat, M. G., Pitman, A. J., Knutti, R., and Wilby, R. L.: Allowable CO<sub>2</sub> emissions based on regional and  
1031 impact-related climate targets, *Nature*, 529, 477–83, <https://doi.org/10.1038/nature16542>, 2016.
- 1032 Sera, F., Armstrong, B., Tobias, A., Vicedo-Cabrera, A. M., Åström, C., Bell, M. L., Chen, B.-Y., de Sousa Zanotti Stagliorio  
1033 Coelho, M., Matus Correa, P., Cruz, J. C., Dang, T. N., Hurtado-Diaz, M., Do Van, D., Forsberg, B., Guo, Y. L., Guo, Y.,  
1034 Hashizume, M., Honda, Y., Iñiguez, C., Jaakkola, J. J. K., Kan, H., Kim, H., Lavigne, E., Michelozzi, P., Ortega, N. V., Osorio,  
1035 S., Pascal, M., Ragetli, M. S., Rytty, N. R. I., Saldiva, P. H. N., Schwartz, J., Scortichini, M., Seposo, X., Tong, S., Zanobetti,  
1036 A., and Gasparrini, A.: How urban characteristics affect vulnerability to heat and cold: a multi-country analysis, *Int. J.*  
1037 *Epidemiol.*, 48, 1101–1112, <https://doi.org/10.1093/ije/dyz008>, 2019.
- 1038 Sharma, A., Wuebbles, D. J., and Kotamarthi, R.: The Need for Urban-Resolving Climate Modeling Across Scales, *AGU*  
1039 *Adv.*, 2, <https://doi.org/10.1029/2020AV000271>, 2021.
- 1040 Sharma, R., Hooyberghs, H., Lauwaet, D., and De Ridder, K.: Urban Heat Island and Future Climate Change-Implications for  
1041 Delhi's Heat, *J Urban Health*, 96, 235–251, <https://doi.org/10.1007/s11524-018-0322-y>, 2019.

- 1042 [Shen, C., Shen, A., Cui, Y., Chen, X., Liu, Y., Fan, Q., Chan, P., Tian, C., Wang, C., Lan, J., Gao, M., Li, X., and Wu, J.:](#)  
1043 [Spatializing the roughness length of heterogeneous urban underlying surfaces to improve the WRF simulation-part I: A review](#)  
1044 [of morphological methods and model evaluation, Atmos. Environ., 270, 118874,](#)  
1045 <https://doi.org/10.1016/j.atmosenv.2021.118874>, 2022.
- 1046 Sillmann, J., Kharin, V. V., Zwiers, F. W., Zhang, X., and Bronaugh, D.: Climate extremes indices in the CMIP5 multimodel  
1047 ensemble: Part 2. Future climate projections, *J. Geophys. Res. Atmospheres*, 118, 2473-2493-2473-2493,  
1048 <https://doi.org/10.1002/jgrd.50188>, 2013.
- 1049 Smid, M., Russo, S., Costa, A. C., Granell, C., and Pebesma, E.: Ranking European capitals by exposure to heat waves and  
1050 cold waves, *Urban Clim.*, 27, 388–402, <https://doi.org/10.1016/j.uclim.2018.12.010>, 2019.
- 1051 Smith, A., Lott, N., and Vose, R.: The Integrated Surface Database: Recent Developments and Partnerships, *Bull. Am.*  
1052 *Meteorol. Soc.*, 92, 704–708, <https://doi.org/10.1175/2011bams3015.1>, 2011.
- 1053 Suarez-Gutierrez, L., Müller, W. A., Li, C., and Marotzke, J.: Dynamical and thermodynamical drivers of variability in  
1054 European summer heat extremes, *Clim. Dyn.*, 54, 4351–4366, <https://doi.org/10.1007/s00382-020-05233-2>, 2020.
- 1055 Sunyer, M. A., Hundedcha, Y., Lawrence, D., Madsen, H., Willems, P., Martinkova, M., Vormoor, K., Bürger, G., Hanel, M.,  
1056 Kriaučiūnienė, J., Loukas, A., Osuch, M., and Yücel, I.: Inter-comparison of statistical downscaling methods for projection of  
1057 extreme precipitation in Europe, *Hydrol. Earth Syst. Sci.*, 19, 1827–1847, <https://doi.org/10.5194/hess-19-1827-2015>, 2015.
- 1058 Taranu, I. S., Somot, S., Alias, A., Boé, J., and Delire, C.: Mechanisms behind large-scale inconsistencies between regional  
1059 and global climate model-based projections over Europe, *Clim. Dyn.*, <https://doi.org/10.1007/s00382-022-06540-6>, 2022.
- 1060 [Tewari, M., Yang, J., Kusaka, H., Salamanca, F., Watson, C., and Treinish, L.: Interaction of urban heat islands and heat waves](#)  
1061 [under current and future climate conditions and their mitigation using green and cool roofs in New York City and Phoenix,](#)  
1062 [Arizona, Environ. Res. Lett., 14, 034002, https://doi.org/10.1088/1748-9326/aaf431](#), 2019.
- 1063 Thompson, R., Landeg, O., Kar-Purkayastha, I., Hajat, S., Kovats, S., and O’Connell, E.: Heatwave Mortality in Summer 2020  
1064 in England: An Observational Study, *Int. J. Environ. Res. Public Health*, 19, 6123, <https://doi.org/10.3390/ijerph19106123>,  
1065 2022.
- 1066 UN-Habitat: Cities and Climate Change, 0 ed., Routledge, <https://doi.org/10.4324/9781849776936>, 2011.
- 1067 [Vaneckova, P., Neville, G., Tippet, V., Aitken, P., FitzGerald, G., and Tong, S.: Do Biometeorological Indices Improve](#)  
1068 [Modeling Outcomes of Heat-Related Mortality?. J. Appl. Meteorol. Climatol., 50, 1165-1176-1165-1176,](#)  
1069 <https://doi.org/10.1175/2011JAMC2632.1>, 2011.
- 1070 Vargas Zeppetello, L. R., Raftery, A. E., and Battisti, D. S.: Probabilistic projections of increased heat stress driven by climate  
1071 change, *Commun. Earth Environ.*, 3, 183, <https://doi.org/10.1038/s43247-022-00524-4>, 2022.
- 1072 Vautard, R., Gobiet, A., Jacob, D., Belda, M., Colette, A., Déqué, M., Fernández, J., García-Díez, M., Goergen, K., Güttler,  
1073 I., Halenka, T., Karacostas, T., Katragkou, E., Keuler, K., Kotlarski, S., Mayer, S., van Meijgaard, E., Nikulin, G., Patarčić,  
1074 M., Scinocca, J., Sobolowski, S., Suklitsch, M., Teichmann, C., Warrach-Sagi, K., Wulfmeyer, V., and Yiou, P.: The  
1075 simulation of European heat waves from an ensemble of regional climate models within the EURO-CORDEX project, *Clim.*  
1076 *Dyn.*, 41, 2555–2575, <https://doi.org/10.1007/s00382-013-1714-z>, 2013.
- 1077 Vautard, R., Kadygrov, N., Iles, C., Boberg, F., Buonomo, E., Bülow, K., Coppola, E., Corre, L., Meijgaard, E., Nogherotto,  
1078 R., Sandstad, M., Schwingshackl, C., Somot, S., Aalbers, E., Christensen, O. B., Ciarlo, J. M., Demory, M.-E., Giorgi, F.,

- 1079 Jacob, D., Jones, R. G., Keuler, K., Kjellström, E., Lenderink, G., Levvasseur, G., Nikulin, G., Sillmann, J., Solidoro, C.,  
1080 Sørland, S. L., Steger, C., Teichmann, C., Warrach-Sagi, K., and Wulfmeyer, V.: Evaluation of the Large EURO-CORDEX  
1081 Regional Climate Model Ensemble, *J. Geophys. Res. Atmospheres*, 126, <https://doi.org/10.1029/2019jd032344>, 2021.
- 1082 Vogel, M. M., Orth, R., Cheruy, F., Hagemann, S., Lorenz, R., Hurk, B. J. J. M., and Seneviratne, S. I.: Regional amplification  
1083 of projected changes in extreme temperatures strongly controlled by soil moisture-temperature feedbacks, *Geophys. Res. Lett.*,  
1084 44, 1511–1519–1511–1519, <https://doi.org/10.1002/2016GL071235>, 2017.
- 1085 [Walters, D., Baran, A. J., Boutle, I., Brooks, M., Earnshaw, P., Edwards, J., Furtado, K., Hill, P., Lock, A., Manners, J.,  
1086 Morcrette, C., Mulcahy, J., Sanchez, C., Smith, C., Stratton, R., Tennant, W., Tomassini, L., Van Weverberg, K., Vosper, S.,  
1087 Willett, M., Browse, J., Bushell, A., Carslaw, K., Dalvi, M., Essery, R., Gedney, N., Hardiman, S., Johnson, B., Johnson, C.,  
1088 Jones, A., Jones, C., Mann, G., Milton, S., Rumbold, H., Sellar, A., Ujiie, M., Whittall, M., Williams, K., and Zerroukat, M.:  
1089 The Met Office Unified Model Global Atmosphere 7.0/7.1 and JULES Global Land 7.0 configurations, \*Geosci. Model Dev.\*,  
1090 12, 1909–1963, <https://doi.org/10.5194/gmd-12-1909-2019>, 2019.](https://doi.org/10.5194/gmd-12-1909-2019)
- 1091 Ward, K., Lauf, S., Kleinschmit, B., and Endlicher, W.: Heat waves and urban heat islands in Europe: A review of relevant  
1092 drivers, *Sci Total Env.*, 569–570, 527–539, <https://doi.org/10.1016/j.scitotenv.2016.06.119>, 2016.
- 1093 Wartenburger, R., Hirschi, M., Donat, M. G., Greve, P., Pitman, A. J., and Seneviratne, S. I.: Changes in regional climate  
1094 extremes as a function of global mean temperature: an interactive plotting framework, *Geosci. Model Dev.*, 10, 3609–3634,  
1095 <https://doi.org/10.5194/gmd-10-3609-2017>, 2017.
- 1096 [White, R. H., Anderson, S., Booth, J. F., Braich, G., Draeger, C., Fei, C., Harley, C. D. G., Henderson, S. B., Jakob, M., Lau,  
1097 C.-A., Mareshet Admasu, L., Narinesingh, V., Rodell, C., Roocroft, E., Weinberger, K. R., and West, G.: The unprecedented  
1098 Pacific Northwest heatwave of June 2021, \*Nat. Commun.\*, 14, 727, <https://doi.org/10.1038/s41467-023-36289-3>, 2023.](https://doi.org/10.1038/s41467-023-36289-3)
- 1099 Wouters, H., De Ridder, K., Poelmans, L., Willems, P., Brouwers, J., Hosseinzadehtalaei, P., Tabari, H., Vanden Broucke, S.,  
1100 van Lipzig, N. P. M., and Demuzere, M.: Heat stress increase under climate change twice as large in cities as in rural areas: A  
1101 study for a densely populated midlatitude maritime region, *Geophys. Res. Lett.*, 44, 8997–9007,  
1102 <https://doi.org/10.1002/2017gl074889>, 2017.
- 1103 Yang, J., Zhou, M., Ren, Z., Li, M., Wang, B., Liu, D. L., Ou, C.-Q., Yin, P., Sun, J., Tong, S., Wang, H., Zhang, C., Wang,  
1104 J., Guo, Y., and Liu, Q.: Projecting heat-related excess mortality under climate change scenarios in China, *Nat. Commun.*, 12,  
1105 1039, <https://doi.org/10.1038/s41467-021-21305-1>, 2021.
- 1106 [Zachariah, M., Philip, S., Pinto, I., Vahlberg, M., Singh, R., Otto, F., Barnes, C., and Kimutai, J.: Extreme heat in North  
1107 America, Europe and China in July 2023 made much more likely by climate change, Imperial College London,  
1108 <https://doi.org/10.25561/105549>, 2023.](https://doi.org/10.25561/105549)
- 1109 Zhao, Y., Ducharme, A., Sultan, B., Braconnot, P., and Vautard, R.: Estimating heat stress from climate-based indicators:  
1110 present-day biases and future spreads in the CMIP5 global climate model ensemble, *Environ. Res. Lett.*, 10, 084013–084013,  
1111 <https://doi.org/10.1088/1748-9326/10/8/084013>, 2015.
- 1112 Zheng, Z., Zhao, L., and Oleson, K. W.: Large model structural uncertainty in global projections of urban heat waves, *Nat*  
1113 *Commun*, 12, 3736, <https://doi.org/10.1038/s41467-021-24113-9>, 2021.
- 1114 Zittis, G., Hadjinicolaou, P., Almazroui, M., Bucchignani, E., Driouech, F., El Rhaz, K., Kurnaz, L., Nikulin, G., Ntoumos,  
1115 A., Ozturk, T., Proestos, Y., Stenchikov, G., Zaaboul, R., and Lelieveld, J.: Business-as-usual will lead to super and ultra-  
1116 extreme heatwaves in the Middle East and North Africa, *Npj Clim. Atmospheric Sci.*, 4, 20, [https://doi.org/10.1038/s41612-  
1117 021-00178-7](https://doi.org/10.1038/s41612-021-00178-7), 2021.

